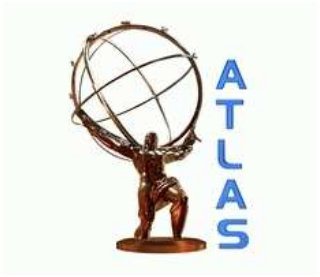

ATLAS NOTE

ATL-PHYS-PUB-2009-000

May 12, 2009

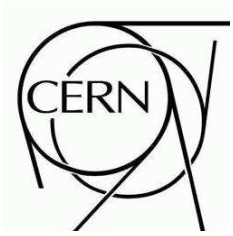

Trigger and Analysis Strategies for B_s^0 Oscillation Measurements in Hadronic Decay Channels

The ATLAS Collaboration[1)]

This note is part of CERN-OPEN-2008-020. This version of the note should not be cited: all citations should be to CERN-OPEN-2008-020.

ATL-PHYS-PUB-2009-052
13 May 2009

Abstract

The capabilities of measuring B_s^0 oscillations in proton-proton interactions with the ATLAS detector at the Large Hadron Collider are evaluated. B_s^0 candidates in the $D_s^- \pi^+$ and $D_s^- a_1^+$ decay modes from semileptonic exclusive events are simulated and reconstructed using a detailed detector description and the ATLAS software chain. For the measurement of the oscillation frequency a Δm_s sensitivity limit of 29.6 ps^{-1} and a five standard deviation measurement limit of 20.5 ps^{-1} are derived from unbinned maximum likelihood amplitude fits for an integrated luminosity of 10 fb^{-1} . The initial flavour of the B_s^0 meson is tagged exclusively with opposite-side leptons. Trigger strategies are proposed for scenarios of different instantaneous luminosities in order to maximise the signal channel trigger efficiencies.

[1)]This note prepared by S. Ben Ami, B. Epp, P. Jussel, E. Kajomovitz, J. Kirk, E. Kneringer, M. Pontz, H. von Radziewski, Y. Rozen, T. Stahl and W. Walkowiak

1 Introduction

As tests of the Standard Model the CP–violation parameter $\sin(2\beta)$ will be measured with high precision (at the percent level) as well as properties of the B_s^0-meson system, like the mass difference of the two mass eigenstates Δm_s, the lifetime difference $\Delta\Gamma_s/\Gamma_s$ and the weak mixing phase ϕ_s induced by CP-violation, with $\phi_s \approx 2\lambda^2\eta$ in the Wolfenstein parametrisation. The different masses of the CP–eigenstates B_s^L (CP–even) and B_s^H (CP–odd) give rise to B_s mixing. The observed B_s^0 and $\bar{B}_s^0$ particles are linear combinations of these eigenstates, where transitions are allowed due to non–conservation of flavour in weak–current interactions and will occur with a frequency proportional to Δm_s. B_s^0 oscillations have been observed at the Fermilab Tevatron collider by the CDF collaboration [1] measuring a value of $\Delta m_s = (17.77 \pm 0.10\,(\text{stat}) \pm 0.07\,(\text{sys}))\,\text{ps}^{-1}$ and D0 collaboration [2] reporting a two-sided bound on the B_s^0 oscillation frequency with a range of $17\ \text{ps}^{-1} < \Delta m_s < 21\ \text{ps}^{-1}$. Both results are consistent with Standard Model expectations [3]. In ATLAS, the Δm_s measurement is an important baseline for the B-physics program and an essential ingredient for a precise determination of the phase ϕ_s. CP–violation in B_s^0-$\bar{B}_s^0$ mixing is a prime candidate for the discovery of non–standard–model physics. For the channel $B_s^0 \to J/\psi\phi$, which has a clean experimental signature, a very small CP-violating asymmetry is predicted in the Standard Model. The measurement of any sizeable effect of the weak–interaction–induced phase ϕ_s in the CKM matrix, which lies above the predicted value, would indicate that processes beyond the Standard Model are involved. Furthermore, the determination of important parameters in the B_s^0 meson system will be valuable input for flavour dynamics in the Standard Model and its extensions.

In this note an estimation of the sensitivity to measure the B_s^0-$\bar{B}_s^0$ oscillation frequency with the ATLAS detector is presented. The signal channels considered are the hadronic decay channels $B_s^0 \to D_s^- \pi^+$ and $B_s^0 \to D_s^- a_1^+$ with $D_s^- \to \phi\pi^-$ followed by $\phi \to K^+K^-$. In the case of $B_s^0 \to D_s^- a_1^+$ the a_1^+ decays as $a_1^+ \to \rho\pi^+$ with $\rho \to \pi^+\pi^-$. Including the sub-decay $D_s^- \to K^{*0}K^-$ [4] would increase the event statistics by about 30%. However, for these sub-channels, which require an additional trigger signature, the increase of the overall trigger rate would be unacceptable. Detailed information of the signal and the exclusive background channels is given in Section 2. The high event rate at the Large Hadron Collider (LHC) imposes very selective requirements onto the B-physics trigger strategies, reducing the rate by about six orders of magnitude for recording events. Since an initial "low-luminosity" running period is scheduled with a luminosity starting at $10^{31}\ \text{cm}^{-2}\text{s}^{-1}$ and rising to $2 \cdot 10^{33}\ \text{cm}^{-2}\text{s}^{-1}$, followed later on by the design luminosity of the LHC of $10^{34}\ \text{cm}^{-2}\text{s}^{-1}$, the B-trigger must be flexible enough to cope with the increasing luminosity conditions. The overall B-trigger strategy as well as the different strategies dealing with the luminosity scenarios in the initial running periods are discussed in Section 3. An important part of the mixing measurement is to identify the flavour at production, i.e., whether the observed B_s meson initially contained a b or a $\bar{b}$ quark. A detailed description of an opposite-side lepton flavour tag and of the various sources of the wrong tag fractions is given in Section 4. The selection of B_s^0 candidates with kinematic cuts as well as mass resolutions of the B_s^0, are explained and shown in Section 5. A luminosity of $10^{33}\ \text{cm}^{-2}\text{s}^{-1}$ and no pileup is considered for the detailed analysis of signal and background channels. Strategies for lower and higher luminosities are also discussed in the same section. The results of the signal-candidate selection are used as input to a toy Monte Carlo simulation generating a sample of B_s^0 candidates, which is used for the amplitude fit method [5] to obtain the Δm_s measurement limits. The construction of the likelihood function, the Monte Carlo sample and the extraction of the Δm_s sensitivity are discussed in Section 6.

2 Simulated Data Samples

Simulated b-quark pairs are generated using PYTHIA [6], with the $\bar{b}$-quark required to decay to one of the specified signal channels. The b-quark decays semileptonically producing a muon with $p_T > 6$ GeV

within $|\eta| < 2.5$. Details on generation, simulation and reconstruction of the simulated data samples are given in the introduction of the B-chapter [7].

In addition to the simulated signal samples $B_s^0 \to D_s^-(\phi\pi^-)\pi^+$ and $B_s^0 \to D_s^-(\phi\pi^-)a_1^+$, corresponding exclusive background channels that give an irreducible contribution to the selected B_s^0 signal were investigated. Two B_d^0 decay channels, $B_d^0 \to D^-\pi^+/a_1^+$ and $B_d^0 \to D_s^+\pi^-/a_1^-$, and one B_s^0 channel, $B_s^0 \to D_s^{*-}\pi^+/a_1^+$, were simulated for both hadronic decay channels. The dedicated trigger studies described in Section 3 require additional samples, such as the inclusive background channels $b\bar{b} \to \mu 6X$, $b\bar{b} \to \mu 4X$ and $c\bar{c} \to \mu 4X$ containing semileptonic b or c decays requiring one muon with a generated $p_T > 4$ GeV (or 6 GeV) and further decay products (X). Also, one particular signal sample (as a choice $B_s^0 \to D_s^- a_1^+$) requiring one muon with a generated $p_T > 4$ GeV (identified by $(\mu 4)$) is used for the trigger studies. A sample of minimum bias events is used for the determination of overall trigger rates. See Table 1 for the number of events generated and the cross-sections calculated from the values given by PYTHIA and the appropriate branching ratios [8]. Errors on the cross-sections include statistical errors and contributions from the uncertainties on the branching ratios.

Effects of pileup and B-meson mixing were not included in the simulation of any of the samples.

Table 1: Number of events generated and calculated cross-sections for the different signal and exclusive background simulated data samples for the $B_s^0 \to D_s^-\pi^+$ and $B_s^0 \to D_s^- a_1^+$ analysis and particular samples used for dedicated trigger studies. Branching ratios for particle decays into final states are included. *)The branching fraction has not been measured yet, only an upper limit exists.

	Channel	Events	Cross-section [pb]
Signal	$B_s^0 \to D_s^-\pi^+$	88 450	10.4 ± 3.5
	$B_s^0 \to D_s^- a_1^+$	98 450	5.8 ± 3.2
Background	$B_d^0 \to D_s^+\pi^-$	43 000	0.2 ± 0.1
	$B_d^0 \to D^-\pi^+$	41 000	6.2 ± 1.1
	$B_s^0 \to D_s^{*-}\pi^+$	40 500	9.1 ± 2.8
	$B_d^0 \to D_s^+ a_1^-$	50 000	< 8.9 *)
	$B_d^0 \to D^- a_1^+$	50 000	3.7 ± 2.1
	$B_s^0 \to D_s^{*-} a_1^+$	100 000	12.1 ± 2.7
Trigger	$B_s^0 \to D_s^- a_1^+$ $(\mu 4)$	50 000	13.6 ± 7.6
	$b\bar{b} \to \mu 6X$	242 150	$(6.14 \pm 0.02) \cdot 10^6$
	$b\bar{b} \to \mu 4X$	98 450	$(19.08 \pm 0.30) \cdot 10^6$
	$c\bar{c} \to \mu 4X$	44 750	$(26.28 \pm 0.09) \cdot 10^6$
	minimum bias	2 623 060	$70 \cdot 10^9$

3 Trigger Strategies

The trigger strategy used for the $B_s^0 \to D_s^-\pi^+$ and $B_s^0 \to D_s^- a_1^+$ channels is to identify the $D_s^\pm$ decaying to $\phi(\to K^+K^-)\,\pi$, which is common to both decay channels. At level one (LVL1) a muon is required to enrich the content of the triggered data sample with B-events. The high level trigger (HLT) is split into level two (LVL2) and Event Filter (EF). A search for a $D_s^\pm$ is performed following one of two strategies. The first method, the FullScan approach, performs reconstruction of tracks within the entire Inner Detector. It is an efficient method, but time consuming and its feasibility depends on the background event rate. The second method performs track reconstruction in a limited volume of the Inner Detector only, which is defined by a low-p_T jet region of interest (RoI) identified at LVL1. This RoI-based method

is faster but there is a loss in efficiency due to the requirement of a LVL1 jet RoI in the event and the geometrical restriction to the RoI.

The increase of the luminosity after LHC startup affects the trigger in two ways: the trigger rates for the jet and muon trigger will increase, seeding the HLT $D_s^{\pm}$ algorithm more frequently, and combinatorial background from pileup affects the performance of the selection algorithm. Therefore, trigger menus corresponding to different LHC luminosities are discussed in Sections 3.4 to 3.6.

The trigger efficiencies are presented for the $B_s^0 \to D_s^- a_1^+$ channel. Results for the $B_s^0 \to D_s^- \pi^+$ channel are expected to be similar within a few percent (see Section 3.2).

3.1 LVL1 Trigger Selection

The ATLAS hardware allows three LVL1 low-p_T muon trigger thresholds to be defined at once, which can only be adjusted between runs by reconfiguring the lookup tables implemented in the muon trigger firmware. In order to study more than three thresholds we investigated the two available, pre-defined menus (named A and B) with respect to the low-p_T muon trigger thresholds[2)].

The three implemented low-p_T thresholds for trigger menu A are: 0 GeV[3)] (named `MU00`), 5 GeV (`MU05`) and 6 GeV (`MU06`). For trigger menu B, the three low-p_T thresholds are 6 GeV (`MU06`), 8 GeV (`MU08`), and 10 GeV (`MU10`). Figure 1 shows the efficiencies of the low-p_T LVL1 muon trigger signatures as a function of the true p_T of the muon with the highest p_T in the event.

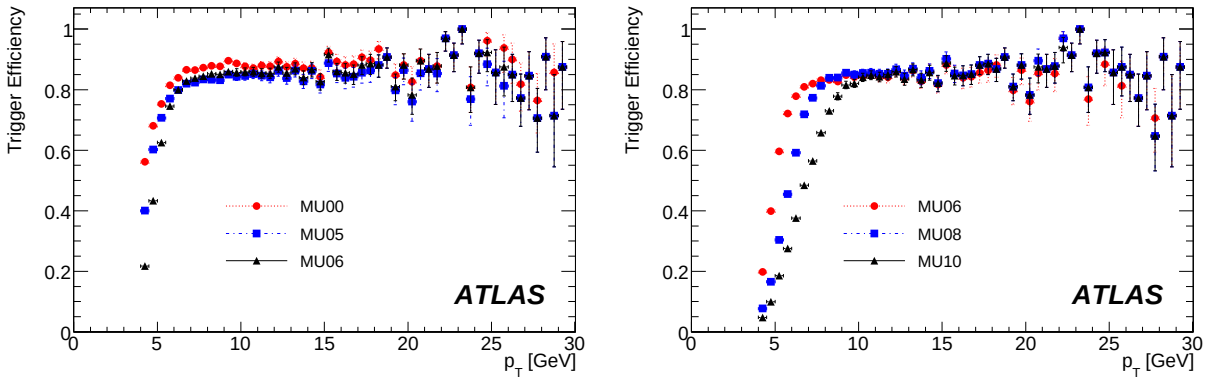

(a) Thresholds for menu A [9]

(b) Thresholds for menu B

Figure 1: Muon trigger efficiency as a function of the true p_T of the muon with the highest p_T in the event for the $B_s^0 \to D_s^- a_1^+(\mu 4)$ for (a) trigger menu A and (b) trigger menu B.

The LVL1 trigger efficiency depends strongly on the threshold chosen for the transverse momentum of the muon as shown in Table 2. Note that there is a discrepancy between the `MU06` efficiencies from both trigger menus, which will be taken as a systematic uncertainty of the current implementation. Although these dedicated trigger studies have been performed with the $B_s^0 \to D_s^- a_1^+$ sample, the LVL1 efficiencies for $B_s^0 \to D_s^- \pi^+(\mu 6)$ have been checked and agree well with those in Table 2.

The input to the LVL1 calorimeter trigger is a set of $\sim$7 200 trigger towers with granularity $\Delta\phi \times \Delta\eta \approx 0.1 \times 0.1$ formed by the analogue summation of calorimeter cells. There are separate sets of

[2)] All presented trigger thresholds are meant to be inclusive, i.e. to include all events fulfilling a trigger signature with a p_T threshold equal to or higher than the indicated one.

[3)] This requires a coincidence between the muon chambers without an actual threshold applied. Due to the detector geometry this corresponds to an effective transverse momentum threshold of about 4 GeV.

Table 2: LVL1 muon trigger efficiencies for the signal datasets $B_s^0 \to D_s^- a_1^+(\mu 4)$ and $B_s^0 \to D_s^- a_1^+(\mu 6)$ and the exclusive background samples. The first three lines refer to trigger menu A [9], while the last three lines refer to trigger menu B. For $b\bar{b} \to \mu 4X$, $b\bar{b} \to \mu 6X$ and $c\bar{c} \to \mu 4X$, the Monte Carlo data samples are only available using trigger menu A.

Menu	Threshold	Efficiency [%]				
		$B_s^0 \to D_s^- a_1^+$ $(\mu 4)$	$B_s^0 \to D_s^- a_1^+$ $(\mu 6)$	$b\bar{b} \to \mu 4X$	$b\bar{b} \to \mu 6X$	$c\bar{c} \to \mu 4X$
A	MU00	75.65 ± 0.19	86.77 ± 0.15	71.74 ± 0.14	86.60 ± 0.07	70.42 ± 0.22
	MU05	68.41 ± 0.21	82.60 ± 0.17	63.51 ± 0.15	81.91 ± 0.08	62.05 ± 0.23
	MU06	58.93 ± 0.22	81.90 ± 0.17	52.28 ± 0.16	81.00 ± 0.08	50.44 ± 0.24
B	MU06	61.15 ± 0.22	83.83 ± 0.16	—	—	—
	MU08	44.78 ± 0.22	77.64 ± 0.19	—	—	—
	MU10	34.89 ± 0.21	65.47 ± 0.21	—	—	—

trigger towers for the EM and hadronic calorimeters. The LVL1 jet algorithm employed here uses a cluster of $\Delta\phi \times \Delta\eta$ of approximately 0.4×0.4 (corresponding to 4×4 trigger towers). The projections of the vectors of the energy depositions onto the plane perpendicular to the beam axis (transverse energy, E_T) are summed over both the electromagnetic and the hadronic layers. The jet algorithm moves the cluster template in steps of 0.2 across the $\phi \times \eta$ plane. An RoI is produced if the 4×4 cluster is a local E_T maximum (as defined in [10]) and the cluster E_T sum is greater than the required threshold. The jet RoI is usable if the average number of RoIs per event (RoI multiplicity, see Fig. 2 and Table 3) is small, ideally about 1-2. Clearly, a compromise is required as an increased threshold will reduce the multiplicity, but will also give a reduced efficiency for finding the B jet in an event.

For a transverse energy threshold of 4 GeV, which is implemented to initiate the LVL2 $D_s^{\pm}$ trigger in trigger menus A and B, the jet trigger has an acceptance of $(98.36 \pm 0.06)\,\%$ based on all events in the $B_s^0 \to D_s^- a_1^+$ sample.

Table 3: Mean and root mean square of the RoI multiplicity distributions (Figure 2) for the background samples as a function of the jet RoI transverse energy (E_T) threshold [9]. Only RoIs with $\eta < 2.4$ have been taken into account. A strong anticorrelation between the E_T threshold and the mean RoI multiplicity is observed.

Threshold	$b\bar{b} \to \mu 4X$		$b\bar{b} \to \mu 6X$		$c\bar{c} \to \mu 4X$	
[GeV]	Mean	RMS	Mean	RMS	mean	RMS
4	2.847	1.746	2.883	1.754	3.235	1.759
5	1.301	1.244	1.441	1.295	1.643	1.300
6	0.703	0.952	0.881	1.046	0.998	1.048
7	0.454	0.786	0.634	0.911	0.703	0.900

3.2 LVL2 Trigger Selection

The first step of LVL2 is to confirm the LVL1 muon trigger decision using more precise muon momentum measurement. Secondly, information from Inner Detector and muon chambers are combined to give a further improvement in the momentum measurement.

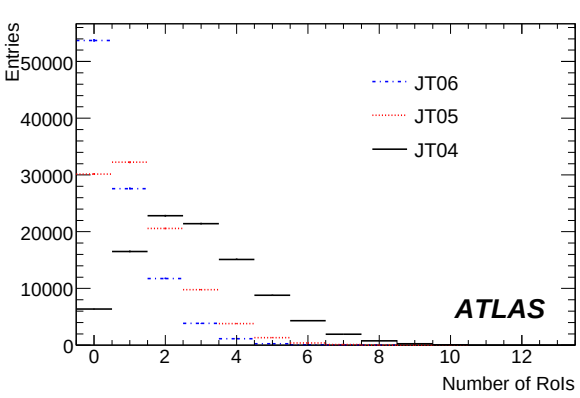

(a) $b\bar{b} \to \mu 4X$

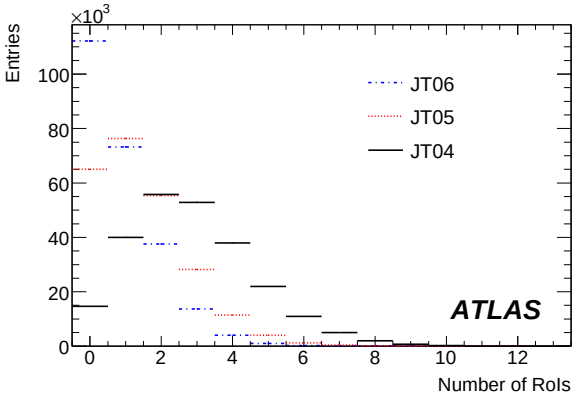

(b) $b\bar{b} \to \mu 6X$

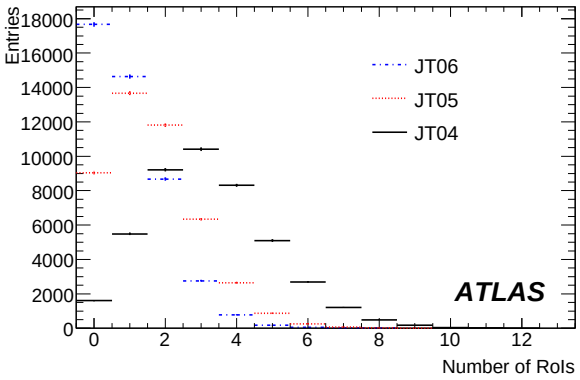

(c) $c\bar{c} \to \mu 4X$

Figure 2: RoI multiplicity distributions for the background samples (a) for $b\bar{b} \to \mu 4X$, (b) for $b\bar{b} \to \mu 6X$ and (c) for $c\bar{c} \to \mu 4X$ as a function of the jet RoI energy threshold [9]. Only RoIs with $\eta < 2.4$ have been taken into account. This corresponds to the requirement that the RoI is to be contained within the solid angle covered by the Inner Detector.

As described above, the LVL2 tracking can be run in either FullScan or RoI-guided modes. In both cases, the same algorithm (named `DsPhiPi`) is used to combine the reconstructed tracks and search first for a ϕ and then for a $D_s^{\pm}$. In the RoI-guided approach tracks are reconstructed in a region $\Delta\phi \times \Delta\eta = 1.5 \times 1.5$ around all jet RoIs with E_T above a certain programmable threshold [11]. A p_T cut of 1.4 GeV is applied to all reconstructed tracks.

Opposite sign track pairs are considered as a ϕ candidate if they pass the following cuts: $|\Delta z| < 3$ mm, where z is the distance along the beam line of the track's point of closest approach to the centre of the detector, $|\Delta\phi| < 0.2$ and $|\Delta\eta| < 0.2$.

The tracks are combined using a K mass hypothesis and a cut around the ϕ mass $m_\phi(\mathrm{PDG}) = 1019.46$ MeV [8] is applied. Track pairs passing the cut are then combined with all other tracks assuming a π mass for the third track. An event is selected if the mass of the track triplet is close to the $D_s^{\pm}$ mass $m_{D_s}(\mathrm{PDG}) = 1968.2$ MeV. The mass cuts used are 1005 MeV $< m_{KK} <$ 1035 MeV for the ϕ candidates and 1908 MeV $< m_{KK\pi} <$ 2028 MeV for the D_s candidates.

The LVL2 track fit masses are shown in Figure 3 and Table 4 for the RoI-guided approach and FullScan. The standard deviations obtained from the Gaussian fits show that the mass cuts used correspond to 3.0 standard deviations for the ϕ mass distribution and 2.8 standard deviations for the $D_s^{\pm}$ mass distribution [9]. The results for the RoI-based approach and those for FullScan agree well.

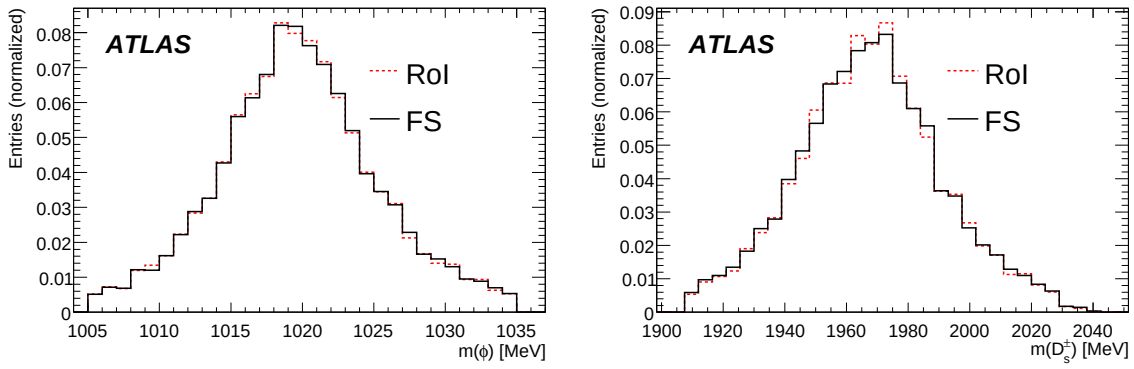

(a) True ϕ candidates

(b) True $D_s^{\pm}$ candidates

Figure 3: LVL2 track fit mass distributions of (a) ϕ and (b) $D_s^{\pm}$ candidates (corresponding to a ϕ or $D_s^{\pm}$ particle from the signal decay in the Monte Carlo truth information) for the FullScan- and RoI-based LVL2 trigger signatures from $B_s^0 \to D_s^- a_1^+$ events fulfilling the respective LVL2 $D_s^{\pm}$ trigger signature and `MU06` [9].

The acceptances of possible trigger strategies up to LVL2 are given in Table 5 for the signal samples and in Table 6 for the background datasets. The LVL2 trigger rates for the $B_s^0 \to D_s^- \pi^+$ channel are expected to be lower by a few percent since the average p_T of the B_s^0 candidates and consequently the average p_T of the D_s candidates is smaller for the $B_s^0 \to D_s^- \pi^+$ channel than for the $B_s^0 \to D_s^- a_1^+$ channel due to different track selections (see Fig. 5 and Section 5.1).

3.3 Event Filter Selection

The muon confirmation at the Event Filter (EF) employs a muon track reconstruction algorithm using muon detector data only, similar to the algorithm used for offline reconstruction.

The EF $D_s^{\pm}$ selection is very similar to that at LVL2. The track reconstruction can be performed in

Table 4: LVL2 track fit masses for the FullScan- and RoI-based LVL2 trigger signatures (only candidates corresponding to a ϕ or $D_s^{\pm}$ particle from the signal decay in the Monte Carlo truth information) from $B_s^0 \to D_s^- a_1^+$ events fulfilling the respective LVL2 $D_s^{\pm}$ trigger and `MU06`. The table shows the results of Gaussian fits within the trigger mass windows to the mass distributions from Fig. 3. The results for both trigger strategies agree within statistical errors.

	FullScan-based LVL2 trigger [9]	RoI-based LVL2 trigger
m(ϕ): mean [MeV]	1019.55 ± 0.05	1019.52 ± 0.05
m(ϕ): std. dev. [MeV]	5.07 ± 0.06	5.04 ± 0.05
m($D_s^{\pm}$): mean [MeV]	1966.9 ± 0.3	1967.0 ± 0.3
m($D_s^{\pm}$): std. dev. [MeV]	21.7 ± 0.3	21.5 ± 0.3

Table 5: Acceptances of LVL2 (RoI and FullScan, FS) for the $B_s^0 \to D_s^- a_1^+$ sample for trigger menus A and B.

Menu A			Menu B		
Trigger scenario	Passes (in %) ($\mu 6$)	Passes (in %) ($\mu 4$)	Trigger scenario	Passes (in %) ($\mu 6$)	Passes (in %) ($\mu 4$)
Events	50 000	50 000		50 000	50 000
`L2_mu0`	85.19±0.16	72.05±0.20	`L2_mu6`	77.13±0.19	35.03±0.21
`L2_mu5`	79.65±0.18	49.39±0.22	`L2_mu8`	45.54±0.22	18.96±0.18
`L2_mu6`	75.66±0.19	34.41±0.21	`L2_mu10`	26.04±0.20	10.91±0.14
FS & `L2_mu0`	32.98±0.21	22.93±0.19	FS & `L2_mu6`	29.99±0.21	12.71±0.15
FS & `L2_mu5`	30.79±0.21	16.75±0.17	FS & `L2_mu8`	19.14±0.18	10.91±0.14
FS & `L2_mu6`	29.38±0.20	12.49±0.15	FS & `L2_mu10`	11.83±0.15	4.92±0.10
RoI & `L2_mu0`	28.74±0.20	19.14±0.18	RoI & `L2_mu6`	26.19±0.20	11.10±0.14
RoI & `L2_mu5`	26.88±0.20	14.26±0.16	RoI & `L2_mu8`	17.09±0.17	7.05±0.12
RoI & `L2_mu6`	25.68±0.20	10.91±0.14	RoI & `L2_mu10`	10.80±0.14	4.56±0.09

Table 6: Acceptances of LVL2 (RoI and FullScan) for the background samples $b\bar{b} \to \mu 4X$, $b\bar{b} \to \mu 6X$ and $c\bar{c} \to \mu 4X$ (trigger menu A).

Trigger scenario	passes (in %) ($b\bar{b} \to \mu 4X$)	passes (in %) ($b\bar{b} \to \mu 6X$)	passes (in %) ($c\bar{c} \to \mu 4X$)
events	98 450	242 150	44 750
FS & `L2_mu0`	2.00±0.05	3.73±0.05	2.71±0.08
FS & `L2_mu5`	1.47±0.04	3.48±0.05	1.93±0.06
FS & `L2_mu6`	1.11±0.03	3.32±0.05	1.43±0.05
RoI & `L2_mu0`	1.73±0.04	3.34±0.05	2.34±0.07
RoI & `L2_mu5`	1.30±0.04	3.12±0.05	1.73±0.06
RoI & `L2_mu6`	1.01±0.03	2.99±0.05	1.32±0.05

FullScan or RoI-guided modes, which share a common EF signature. The search for ϕ and $D_s^{\pm}$ particles currently uses the same mass cuts as at LVL2, even though better mass resolutions are expected for the EF than for LVL2. In the future the mass cuts might be tightened and additional selection cuts will be added as discussed in section 3.5. EF output rates, which are only available for the minimum bias sample, are discussed in the following subsections.

3.4 Trigger Strategies for Early Running

At the lowest luminosities (10^{31} cm^{-2}s^{-1} and 10^{32} cm^{-2}s^{-1}), the trigger selection needs to be as efficient as possible, which means running a loose trigger. To estimate rates and perform timing studies a trigger menu with a different set of muon thresholds [12] is applied to the minimum bias sample. Table 7 shows the expected trigger rates for muons at LVL1 and after confirmation at LVL2. The output rates of the `DsPhiPi` trigger at LVL2 and the EF are given in Table 8 for 10^{31} cm^{-2}s^{-1}. For a luminosity of 10^{33} cm^{-2}s^{-1} and higher, the rates are expected to increase because of event pile-up and cavern background events.

Table 7: Muon rates based on $2.6 \cdot 10^6$ minimum bias events. Rates set in *italics* are based on an interpolation using an exponential approximation of the rate dependence on the muon threshold concerned. Effects caused by event pile-up and cavern-background events are not included.

Luminosity	LVL1				
[cm^{-2}s^{-1}]	L1_MU00		L1_MU06		L1_MU10
10^{31}	1.3 ± 0.02 kHz		480 ± 10 Hz		266 ± 8 Hz
10^{32}	13.0 ± 0.2 kHz		4.8 ± 0.1 kHz		2.7 ± 0.1 kHz
$1 \cdot 10^{33}$	130 ± 2 kHz		48 ± 1 kHz		27 ± 1 kHz
$2 \cdot 10^{33}$	260 ± 4 kHz		96 ± 2 kHz		54 ± 2 kHz
	LVL2				
	L2_mu0	L2_mu5	L2_mu6	L2_mu8	L2_mu10
10^{31}	450 ± 11 Hz	*213* Hz	120 ± 6 Hz	*50* Hz	25 ± 3 Hz
10^{32}	4.5 ± 0.1 kHz	*2.1* kHz	1.20 ± 0.06 kHz	*500* Hz	250 ± 30 Hz
$1 \cdot 10^{33}$	45.0 ± 1.1 kHz	*21* kHz	12.0 ± 0.6 kHz	*5* kHz	2.5 ± 0.3 kHz
$2 \cdot 10^{33}$	90.0 ± 2.2 kHz	*42* kHz	24.0 ± 1.2 kHz	*10* kHz	5.0 ± 0.6 kHz

In addition to the overall allowed output rate, the time constraints of the HLT system are limiting the `DsPhiPi` trigger. The maximum allowed average computing times are 40 ms at LVL2 and 1 s at the EF. Most of the time is taken in the tracking algorithms as can be seen in Table 9 which shows the average CPU time used by the tracking and hypothesis algorithms at LVL2 and EF.

Table 10 summarises the LVL2 efficiencies and the expected numbers for $B_s^0 \to D_s^- a_1^+(\mu 4)$ events before and after the application of event selection cuts in the analysis as well as the estimated LVL2 and EF trigger rates for different luminosity scenarios and different trigger choices. The L2 and EF output rates shown in this table are deduced from the rate information given in Tables 7 and 8. The LVL2 muon trigger efficiency estimates presented in Table 10 are based on the LVL2 results obtained with the $B_s^0 \to D_s^- a_1^+(\mu 4)$ sample shown in Table 5.

At 10^{31} cm^{-2}s^{-1}, once the improvements discussed in Section 3.5 have been applied to the EF algorithms, it should be possible to run the FullScan-based trigger at the LVL1 4 GeV muon rate and to remain within the constraints given by available trigger resources. As the luminosity is increased to 10^{32} cm^{-2}s^{-1}, we will need to raise the muon threshold for the FullScan-based trigger or to move to a

Table 8: Output rates for the `DsPhiPi` trigger based on $2.6 \cdot 10^6$ minimum bias events at 10^{31} cm^{-2}s^{-1}. Rates set in *italics* are based on an interpolation using the results from Table 7.

	LVL2		EF	
Muon input trigger	RoI	FullScan	RoI	FullScan
L1_MU00	23 ± 3 Hz	31 ± 3 Hz	14 ± 2 Hz	19 ± 2 Hz
L1_MU06	11 ± 2 Hz	13 ± 2 Hz	6.4 ± 1.3 Hz	7.5 ± 1.4 Hz
L2_mu0	15 ± 2 Hz	18 ± 2 Hz	6.1 ± 1.3 Hz	6.9 ± 1.4 Hz
L2_mu5	*9.5* Hz	*9.9* Hz	*4.5* Hz	*4.5* Hz
L2_mu6	6.7 ± 1.3 Hz	6.4 ± 1.3 Hz	3.5 ± 1.0 Hz	3.2 ± 0.9 Hz
L2_mu8	*3.9* Hz	*3.3* Hz	*2.1* Hz	*1.7* Hz
L2_mu10	*2.5* Hz	*2.0* Hz	*1.2* Hz	*0.9* Hz

Table 9: Average CPU times on an HLT computing node (Dual core Intel(R) Xeon(R) CPU 5160 @ 3.00 GHz) using 900 $b\bar{b} \rightarrow \mu 6X$ events.

		Algorithm	Time/RoI	Time/event
LVL2	tracking	Idscan_RoI	15 ms	23 ms
		Idscan_FullScan		91 ms
	hypothesis	`DsPhiPi`		< 1 ms
Event Filter	tracking	RoI	130 ms	208 ms
		FullScan		470 ms
	hypothesis	`DsPhiPi`		< 1 ms

RoI-based trigger. However, the muon threshold should be kept as low as possible in order to achieve the highest possible trigger efficiency and to allow for as many $B_s^0 \rightarrow D_s^- a_1^+$ events as possible to pass. Compared to earlier publications like [13] the $b\bar{b}$ cross-section as shown in [7] is at the upper limit of what is expected and therefore the muon rates are likely to be overestimated.

3.5 Trigger Strategies for Running at 10^{33} cm^{-2}s^{-1}

At 10^{33} cm^{-2}s^{-1} the trigger needs to remain as efficient as possible while operating within the constraints of the trigger system's resources. The EF output rate is expected to be about 10-20 Hz for B-physics.

The muon rates expected at LVL1 and LVL2 for different thresholds and luminosities are included in Table 7. The LVL2 muon rates are the input rates for the LVL2 tracking algorithms. Using the information on jet RoI multiplicities from Figure 2 and Table 3, the computing times from Table 9 and the muon rates in Table 7, trigger strategies are determined for different luminosities.

For a luminosity of 10^{33} cm^{-2}s^{-1}, a LVL1 trigger muon in combination with the RoI-based D_s trigger will be used. It is planned to use thresholds of 6 GeV for the trigger muon and 5 GeV for the jet RoI trigger. It is clear from Table 8 that in order to run such a trigger the LVL2 and EF selections will have to be tightened. This may be achieved by introducing vertex fitting and by reconstructing the B_s^0 at the EF level.

Preliminary studies at LVL2 show that a requirement for a vertex fit to the 3 tracks of the D_s candidate can achieve a factor 2 rate reduction for a drop in efficiency from 38% to 32%. This estimate is applied to cells marked by $^{\#}$ and † in Table 10. Also, it might be an option to further reduce the rate by tightening

Table 10: LVL2 and EF output rates for minimum bias events, LVL2 trigger efficiencies and numbers of expected $B_s^0 \to D_s^- a_1^+(\mu 4)$ events without or with selection cuts. Rates set in *italics* are estimates based on the interpolated and extrapolated rates given in Table 7. LVL2 output rates marked by † are downscaled by a factor two, the estimated rate reduction for a D_s vertex requirement at LVL2. For EF output rates marked by ‡, an estimated rate reduction factor of 60 accounting for EF B_s^0 reconstruction is applied. (See section 3.5 for details.) The results in the columns "LVL2 eff." and $N_{LVL2\ output}^{B_s^0 \to D_s^- a_1^+}$ (without and with selection cuts applied) are based on the $B_s^0 \to D_s^- a_1^+(\mu 4)$ Monte Carlo data sample. Numbers marked by $^\#$ are corrected for the estimated efficiency loss by a D_s vertex requirement at LVL2. The integrated luminosities and expected event numbers correspond to one year running at the given instantaneous luminosity (10^7 seconds).

$\mathscr{L}$ $[\mathrm{cm}^{-2}\mathrm{s}^{-1}]$	$\int \mathscr{L} dt$ $[\mathrm{pb}]^{-1}$	Trigger set	LVL2 eff. [%]	$N_{LVL2\ output}^{B_s^0 \to D_s^- a_1^+}$ no sel. cuts	$N_{LVL2\ output}^{B_s^0 \to D_s^- a_1^+}$ incl. sel. cuts	LVL2 rate [Hz]	EF rate [Hz]
10^{31}	100	L2mu0FS	22.93 ± 0.19	308	63	18 ± 2	6.9 ± 1.4
		L2mu5FS	16.75 ± 0.17	225	47	*9.9*	*4.5*
		L2mu6FS	12.49 ± 0.15	168	35	6.4 ± 1.3	3.2 ± 0.9
10^{32}	1 000	L2mu6FS	12.49 ± 0.15	1 678	351	64 ± 13	32 ± 9
		L2mu5RoI	14.26 ± 0.16	1 916	267	*95*	*45*
		L2mu6RoI	10.91 ± 0.14	1 466	322	67 ± 13	35 ± 10
10^{33}	10 000	L2mu5RoI	$12.01 \pm 0.13^\#$	$16\,134^\#$	$3\,582^\#$	$475^\dagger$	$7.5^\ddagger$
		L2mu6RoI	$9.19 \pm 0.12^\#$	$12\,344^\#$	$2\,709^\#$	$335 \pm 93^\dagger$	$5.8 \pm 2.0^\ddagger$
		L2mu8RoI	$5.94 \pm 0.10^\#$	$7\,976^\#$	$1\,757^\#$	$196^\dagger$	$3.5^\ddagger$
		L2mu10RoI	$3.84 \pm 0.08^\#$	$5\,159^\#$	$1\,132^\#$	$126^\dagger$	$2.0^\ddagger$
$2 \cdot 10^{33}$	20 000	L2mu6RoI	$9.19 \pm 0.12^\#$	$24\,687^\#$	$5\,418^\#$	$670 \pm 187^\dagger$	$11.7 \pm 4.0^\ddagger$
		L2mu8RoI	$5.94 \pm 0.10^\#$	$15\,953^\#$	$3\,517^\#$	$392^\dagger$	$7.1^\ddagger$
		L2mu10RoI	$3.84 \pm 0.08^\#$	$10\,318^\#$	$2\,264^\#$	$252^\dagger$	$4.1^\ddagger$

the acceptance windows for m_ϕ and m_{D_s} on LVL2, but the resulting rate reduction and the expected signal efficiency loss will need to be studied.

A considerable rate reduction at the EF level may be achieved by reconstructing the B_s^0. A preliminary study using offline selection cuts (see Section 5.1), which have been relaxed to simulate wider mass window and vertexing requirements for the reconstructed particles, has been performed with the $b\bar{b} \to \mu 4X$ and $c\bar{c} \to \mu 4X$ samples. The resulting rate reduction factor, estimated to be approximately 60, is applied to cells marked by ‡ in Table 10. According to this study, the overall trigger and reconstruction efficiency for the $B_s^0 \to D_s^- a_1^+$ signal events will be reduced by about 55%. Although these estimates will need to be confirmed by an implementation of a simplified B_s^0 reconstruction at the EF level, reasonable EF output rates are expected to be achievable.

The numbers of expected $B_s^0 \to D_s^- a_1^+(\mu 4)$ events for 10 fb^{-1} of data for a luminosity of 10^{33} $\mathrm{cm}^{-2}\mathrm{s}^{-1}$ are given in Table 10. It will be necessary to establish a muon trigger threshold as low as possible to maximise the signal event yield.

3.6 Trigger Strategies for Higher Luminosities

As luminosity increases, it is necessary to stay within the limits of the LVL2 trigger processing times and allowable output rates. As Table 10 shows, this will require increasing the muon threshold to 8 GeV or 10 GeV and to add additional trigger elements in the EF as discussed at the end of Section 3.5. Another

option, however a less efficient one, is to prescale the 6 GeV rate before running the track reconstruction.

4 Flavour Tagging

The measurement of B_s^0 oscillations needs the knowledge of the flavour of the B_s^0 meson at production time and at decay time in order to classify events as mixed or not mixed. The tagging algorithm tries to determine the flavour at production time, whereas the decay particles of the signal B_s^0 determine the flavour at decay time. In this analysis soft muon tagging (see B-physics chapter of [4]) is used and the general application on the simulated data samples is shown in Section 4.2 without applying trigger conditions or any selection cut. Tagging results specific for the hadronic channels under investigation including trigger and selection cuts for B_s^0 candidates are given in Section 5.3.

4.1 Soft Muon Tagging

In proton-proton collisions b quarks are produced in pairs leaving the signal B_s^0 and the opposite side b hadron with the opposite flavour. In the case of a semileptonic decay as shown in Fig. 4, the charge of the produced lepton is correlated with the flavour of the signal B_s^0 meson at production time. The charge of the muon with the highest reconstructed p_T is used for the determination of the flavour. Because of the muon trigger, in hadronic B_s^0 decay channels soft muon tagging has a high tagging efficiency $\varepsilon_{tag} = N_{tag}/N_{all}$ limited by the muon reconstruction efficiency. Details on the aspects of muon reconstruction and identification in ATLAS can be found in [14].

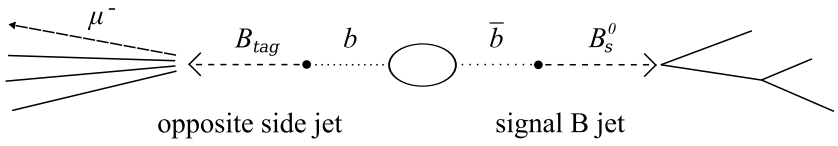

Figure 4: In the case of a signal B_s^0, the associated opposite side b hadron decaying semileptonically produces a negatively charged lepton.

The dilution factor is defined as $D_{tag} = \frac{N_c - N_w}{N_c + N_w}$ where N_c is the number of events correctly tagged and N_w is the number of events with a wrong tag. These wrong tags arise from mixing of the tagging b hadron, muons from decays $b \to c \to \mu$, additional c pairs and various particles decaying into muons. The wrong tag fraction $\omega = N_w/(N_c + N_w)$ is the ratio of wrongly tagged events to all tagged events. As the generation of the simulated data does not include B meson oscillations, mixing of the tagging side hadron is introduced artificially using the integrated mixing probabilities χ_d and χ_s [8]:

$$\chi_d = \frac{\Gamma(B_d^0 \to \bar{B}_d^0 \to \mu^+ X)}{\Gamma(B_d^0 \to \mu^\pm X)} = 0.188 \pm 0.003 \qquad \chi_s = \frac{\Gamma(B_s^0 \to \bar{B}_s^0 \to \mu^+ X)}{\Gamma(B_s^0 \to \mu^\pm X)} = 0.499\,24 \pm 0.000\,03$$

4.2 Application to Signal Samples

In Fig. 5 the transverse momentum of the signal B_s^0 mesons is compared for the two B_s^0 decay channels, the vertical lines show the mean values of the two distributions. This difference arises from the different kinematical configuration due to the condition on all charged final state particles $p_T > 0.5$ GeV at Monte Carlo generation. As $B_s^0 \to D_s^- a_1^+$ has a total number of six final state particles, the mean transverse

momentum of the signal B_s^0 is higher compared to $B_s^0 \to D_s^- \pi^+$ with a total number of four final state particles. The difference in the B_s^0 transverse momentum spectrum is also expected at offline reconstruction level due to the different p_T selection cuts for the π and the a_1 combinations (see Section 5.1). This leads in the case of the $B_s^0 \to D_s^- \pi^+$ sample to an overall wrong tag fraction of $\omega = 20.29 \pm 0.14$ % and in the case of the $B_s^0 \to D_s^- a_1^+$ channel to a wrong tag fraction $\omega = 21.05 \pm 0.11$ %, which is higher compared to the $B_s^0 \to D_s^- \pi^+$ channel (see all events in Table 11 in Section 5.3).

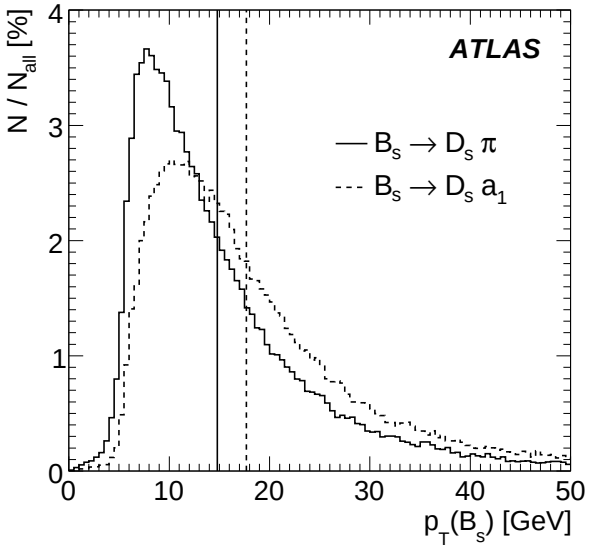

Figure 5: Normalised distributions of signal B_s^0 transverse momentum p_T of the two channels $B_s^0 \to D_s^- \pi^+$ and $B_s^0 \to D_s^- a_1^+$. The vertical lines represent the mean values of the distributions, in the case of $B_s^0 \to D_s^- \pi^+$ the mean is 14.80 ± 0.03 GeV, in the case of $B_s^0 \to D_s^- a_1^+$ 17.68 ± 0.03 GeV. The observed difference is due to the different particle selections.

In Fig. 6 the wrong tag fractions and the sources of these wrong tags are compared for both B_s^0 decays channels. The wrong tag fraction is shown as a function of the tagging muon's transverse momentum $p_T(\mu)$, in Fig. 6(a) for $B_s^0 \to D_s^- \pi^+$ and in Fig. 6(b) for $B_s^0 \to D_s^- a_1^+$. In the regime $p_T(\mu) < 11$ GeV the $B_s^0 \to D_s^- a_1^+$ wrong tag fraction is higher. As mentioned above this difference arises from the different track selections of the two decay channels. In both channels the two main sources of wrong tags are mixing of neutral B mesons on the tagging side and muons from cascade decays $b \to c \to \mu$. As the overall wrong tag fraction is decreasing with the muon p_T, also the part with a wrong tag due to the cascade $b \to c \to \mu$ is decreasing at the same rate. A further source of mistags are additional $c\bar{c}$-pairs. The wrong tag fraction of this part stays about constant with increasing $p_T(\mu)$. A small part of the wrong tag fraction originates from J/ψ, ϕ, ρ, η or τ particles decaying into muons. Additional sources like muons from kaons and pions or hadrons misidentified as muons can be neglected [12].

A $b\bar{b}$ pair produced in proton proton collisions has a transverse momentum equal to zero at first order. Going through fragmentation and hadronisation, the p_T of the signal B_s^0 meson and the opposite side b hadron are still correlated, and therefore a muon coming from a semileptonic decay of the b hadron also is correlated with the signal B_s^0. Hence a muon from a cascade $b \to c \to \mu$ is more likely to pass the LVL1 muon trigger when B_s^0 meson has a higher p_T, leading to the increase in wrong tag fraction with $p_T(B_s^0)$. This behaviour is shown in the Fig. 6(c) and 6(d).

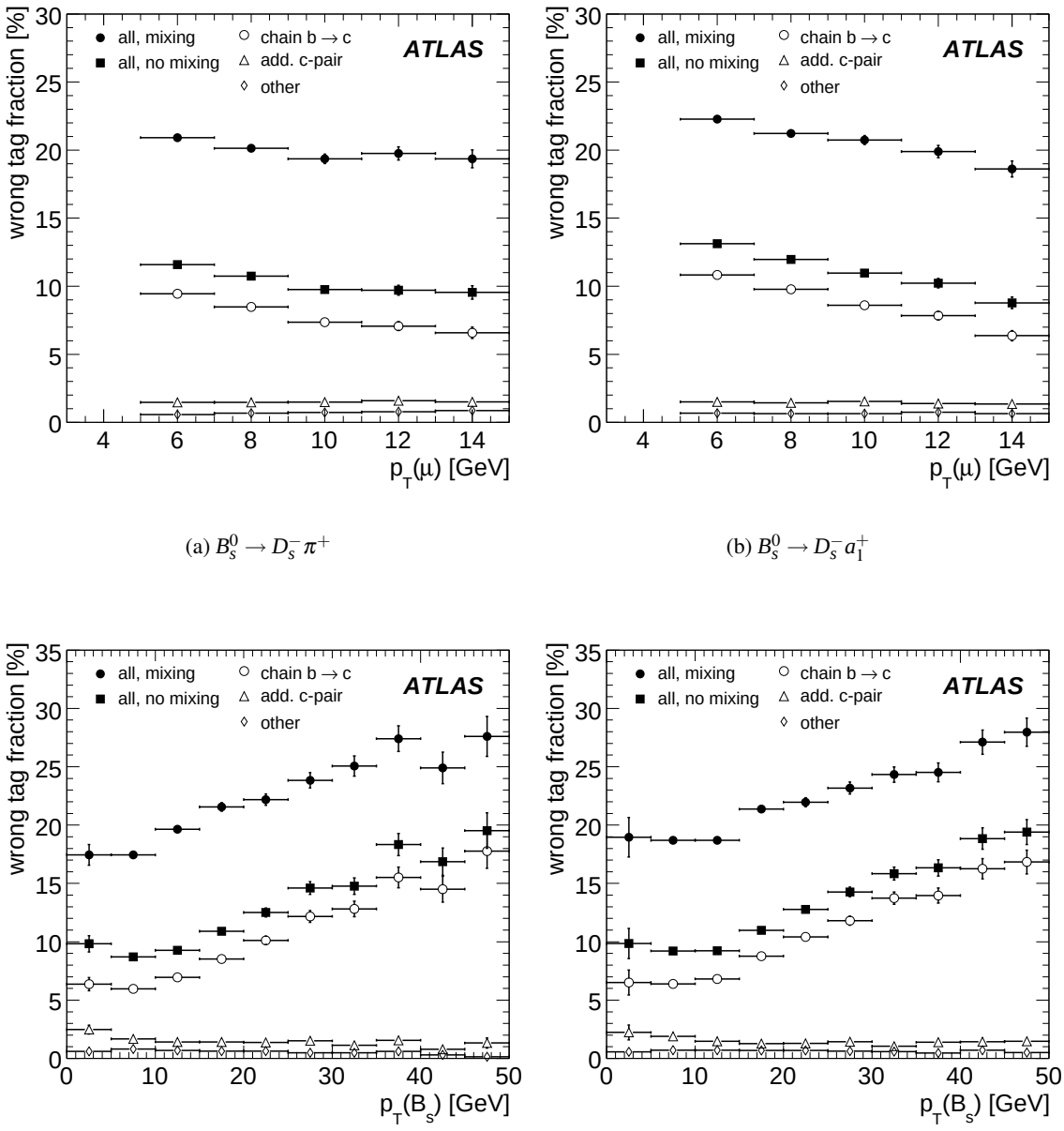

(a) $B_s^0 \to D_s^- \pi^+$

(b) $B_s^0 \to D_s^- a_1^+$

(c) $B_s^0 \to D_s^- \pi^+$

(d) $B_s^0 \to D_s^- a_1^+$

Figure 6: Wrong tag fraction as functions of tagging muons transverse momentum $p_T(\mu)$ in (a) and (b) and wrong tag fractions as functions of signal Monte Carlos B_s^0 transverse momentum $p_T(B_s^0)$ in (c) and (d). The wrong tag fraction is shown with mixing of the tagging side b hadron and without mixing. Without mixing, the different sources of wrong tags are shown. The main contribution is coming from $b \to c \to \mu$ followed by additional c pairs. Additional sources shown are muons coming from J/ψ, ϕ, ρ, η and τ.

4.3 Systematic Uncertainties of Soft Muon Tagging

The calibration of the soft muon tagger will be done with events from the exclusive decay channel $B^+ \to J/\psi(\mu^+\mu^-)K^+$. The high branching ratio and the simple event topology allows the measurement of this channel during the initial luminosity phase at the LHC. Without mixing on the signal side, these events can be used to estimate the systematic uncertainties of soft muon tagging.

For an integrated luminosity of 1 fb^{-1} 160 000 events of the decay channel $B^+ \to J/\psi(\mu^+\mu^-)K^+$ are expected [15] at ATLAS. About 13.5 % events are estimated to have an additional third muon for flavour tagging. Requiring a minimum transverse momentum of 6 GeV for this additional muon, the number of events will be reduced by a factor of three. Assuming that the wrong tag fraction in this channel behaves like in the hadronic B_s^0 decay channels, the expected statistical error of the wrong tag fraction would be of the order of 0.1 % for 1 fb^{-1} integrated luminosity.

5 Event Selection

For the following analysis selecting B_s candidates the default trigger choices are to require MU06 and JT04 trigger elements at LVL1 and to perform a search for the $D_s \to \phi(K^+K^-)\pi$ decay within a jet RoI at LVL2. Resulting event numbers and plots are given for 10 fb^{-1} unless indicated otherwise.

5.1 Signal Event Reconstruction

For the reconstruction of the B_s vertex only tracks with a pseudo-rapidity $|\eta| < 2.5$ are used proceeding via the following steps. The ϕ decay vertex is first reconstructed by considering all pairs of oppositely-charged tracks with $p_T > 1.5$ GeV for both tracks. Kinematic cuts on the angles between the two tracks, $\Delta\varphi_{KK} < 10^\circ$ and $\Delta\theta_{KK} < 10^\circ$, are imposed, where φ denotes the azimuthal angle and θ the polar angle. The two-track vertex is then fitted assigning the kaon mass to both tracks. Combinations passing a fit-probability cut [16] of 1% ($\simeq \chi^2$/dof = 7/1) with the invariant mass within three standard deviations of the nominal ϕ mass are selected as ϕ candidates. The plots in Fig. 7 show the invariant mass distribution for all m_{KK} combinations overlaid with the ϕ candidates matching a generated ϕ from the signal decay (grey filled area) fitted with a single Gaussian function. For the $B_s^0 \to D_s^-\pi^+$ channel the mass resolution is $\sigma_\phi = (4.30 \pm 0.03)$ MeV and for the $B_s^0 \to D_s^- a_1^+$ channel $\sigma_\phi = (4.28 \pm 0.03)$ MeV. This mass window for accepted ϕ candidates is shown by the vertical lines. No trigger selections are applied for the mass plots shown in Fig. 7 to Fig. 9.

From the remaining tracks, a third track with $p_T > 1.5$ GeV is added to all accepted ϕ candidates. The pion mass is assigned to the third track and a three-track vertex is fitted. Three-track vertex candidates which have a fit probability greater than 1% ($\simeq \chi^2$/dof = 12/3) and an invariant mass within three standard deviations of the nominal D_s mass are selected as D_s candidates. The plots in Fig. 8 show the invariant mass distribution for all $m_{KK\pi}$ combinations overlaid with the D_s candidates matching a generated D_s from the signal decay (grey filled area) fitted with a single Gaussian function. For the $B_s^0 \to D_s^-\pi^+$ channel the mass resolution is $\sigma_{D_s} = 17.81 \pm 0.13$ MeV and for the $B_s^0 \to D_s^- a_1^+$ channel $\sigma_{D_s} = 17.92 \pm 0.13$ MeV. The $3\sigma_{D_s}$ mass range for accepted D_s candidates is shown by the vertical lines.

For the $B_s^0 \to D_s^- a_1^+$ channel a search is performed for $a_1^\pm$ candidates using three-particle combinations of charged tracks for events with a reconstructed D_s meson. In a first step ρ^0 mesons are reconstructed from all combinations of two tracks with opposite charges and with $p_T > 0.5$ GeV, each particle in the combination being assigned a pion mass. A kinematic cut $\Delta R_{\pi\pi} = \sqrt{\Delta\phi_{\pi\pi}^2 + \Delta\eta_{\pi\pi}^2} < 0.650$ is used to reduce the combinatorial background. The two selected tracks are then fitted as originating from the same vertex; from the combinations passing a fit probability cut of 1% ($\simeq \chi^2$/dof = 7/1), those with an invariant mass within 400 MeV of the nominal ρ^0 mass are selected as ρ^0 candidates. Next a third track with $p_T > 0.5$ GeV from the remaining charged tracks is added to the ρ^0 candidate, assuming the

pion hypothesis for the extra track. A kinematic cut $\Delta R_{\rho\pi} < 0.585$ is applied. The three tracks are fitted to a common vertex without any mass constraints. Combinations with a fit probability greater than 1% ($\simeq \chi^2$/dof = 12/3) and with an invariant mass within 325 MeV of the nominal a_1 mass are selected as $a_1^{\pm}$ candidates.

The B_s^0 candidates are reconstructed combining the $D_s^{\pm}$ candidates with $a_1^{\pm}$ candidates with opposite charge and different tracks. A six-track vertex fit is performed with mass constraints for the tracks from ϕ and D_s; due to the large a_1 natural width the three tracks from the a_1 are not constrained to the a_1 mass. The total momentum of the B_s^0 vertex is required to point to the primary vertex and the momentum of the D_s vertex to the B_s^0 vertex. Only six-track combinations with a vertex fit probability greater than 1% ($\simeq \chi^2$/dof = 27/12) are considered as B_s^0 candidates.

For the $B_s^0 \to D_s^- \pi^+$ channel for each reconstructed D_s meson a fourth track from the remaining tracks in the event is added. This track is required to have opposite charge with respect to the pion track from the D_s and $p_T > 1$ GeV. The four-track decay vertex is fitted including ϕ and D_s mass constraints, and requiring that the total momentum of the B_s^0 vertex points to the primary vertex and the momentum of D_s vertex points to the B_s^0 vertex. In order to be selected as B_s^0 candidates, the four-track combinations are required to have a vertex fit probability greater than 1% ($\simeq \chi^2$/dof = 20/8).

For both channels, $B_s^0 \to D_s^- \pi^+$ and $B_s^0 \to D_s^- a_1^+$, the signed separation between the reconstructed B_s^0 vertex and the primary vertex is required to be positive (the momentum should not point backward to the parent vertex). To improve the purity of the sample, further cuts are imposed: the proper decay time of the B_s^0 has to be greater than 0.4 ps, the B_s^0 impact parameter (shortest distance of the reconstructed B_s^0 trajectory from the primary vertex in the transverse plane to the reconstructed B_s^0 decay vertex) is required to be smaller than 55 μm and p_T of the B_s^0 must be larger than 10 GeV. The plot in Fig. 9(a) shows the invariant mass distribution for all $m_{KK\pi\pi}$ B_s candidates matching a generated B_s from the signal decay for the $B_s^0 \to D_s^- \pi^+$ channel fitted with a single Gaussian function and giving a mass resolution of $\sigma_{B_s} = 52.80 \pm 0.68$ MeV. For the $B_s^0 \to D_s^- a_1^+$ channel Fig. 9(b) shows the invariant mass distribution for all $m_{KK\pi\pi\pi\pi}$ B_s candidates matching a generated B_s and giving a mass resolution of $\sigma_{B_s} = 40.82 \pm 0.53$ MeV. The difference in the B_s^0 mass resolutions is caused by the p_T spectrum of the π in the $B_s^0 \to D_s^- \pi^+$ decay being harder than the p_T spectra of the three pions in the $B_s^0 \to D_s^- a_1^+$ decay, as the pion momentum resolution is worse for higher p_T. A final mass cut of two standard deviations on the B_s^0 candidates is applied for further analysis (see vertical lines in Fig. 9). For some events more than one B_s^0 candidate is reconstructed and in that case the candidate with the lowest χ^2/dof from the vertex fit is selected for further analysis.

No relevant effects induced by the trigger selections on fit variables of the mass plots or the kinematic distributions of the B_s candidates are found (discussed in Section 6.3). All differences are within the fit errors.

5.2 Background Channels

Two main sources of background are considered: irreducible background coming from a decay channel that closely mimics the B_s^0 signal and combinatorial background coming from random combination of tracks.

5.2.1 Exclusive Background Channels

The exclusive samples listed in Table 1 are used as irreducible background sources. See Table 12 in Section 6 for the numbers of reconstructed candidates after applying the same selection cuts as for the signal samples. The histograms in Fig. 10 show the invariant mass spectrum of reconstructed B_s^0 candidates for the $B_s^0 \to D_s^- \pi^+$ and $B_s^0 \to D_s^- a_1^+$ channel respectively (no trigger selection cut applied). The different contributions are scaled with the cross-section given in Table 1.

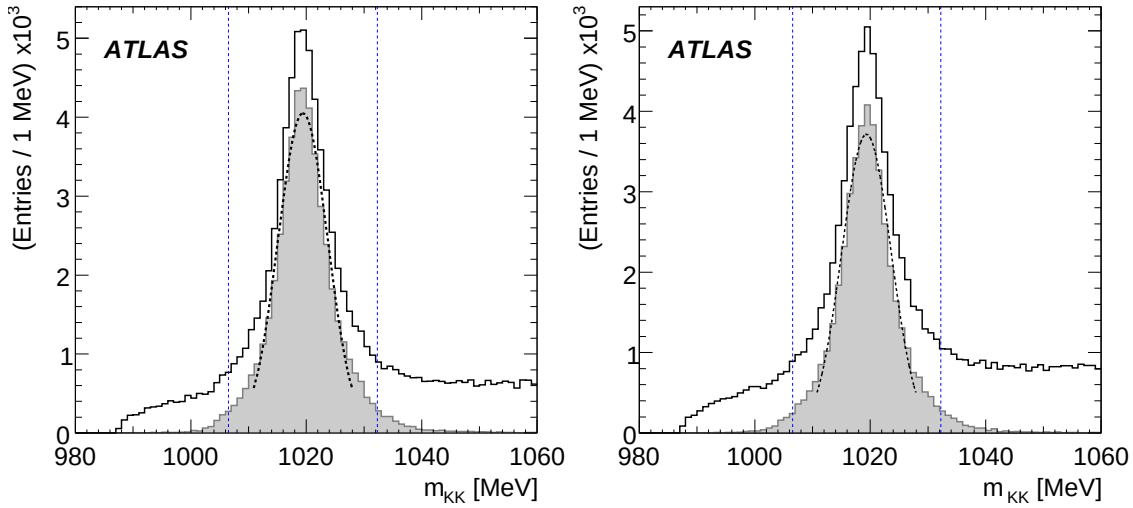

(a) $B_s^0 \to D_s^- \pi^+$ (b) $B_s^0 \to D_s^- a_1^+$

Figure 7: Reconstructed mass m_{KK} for all combinations within the signal sample (black line) and KK candidates corresponding to a ϕ particle from the signal decay in the Monte Carlo truth information (grey filled). The standard deviation obtained from a fit within two standard deviations of a Gaussian function (dashed) to the distribution defines the three standard deviation cut range (vertical dashed). No trigger conditions are applied.

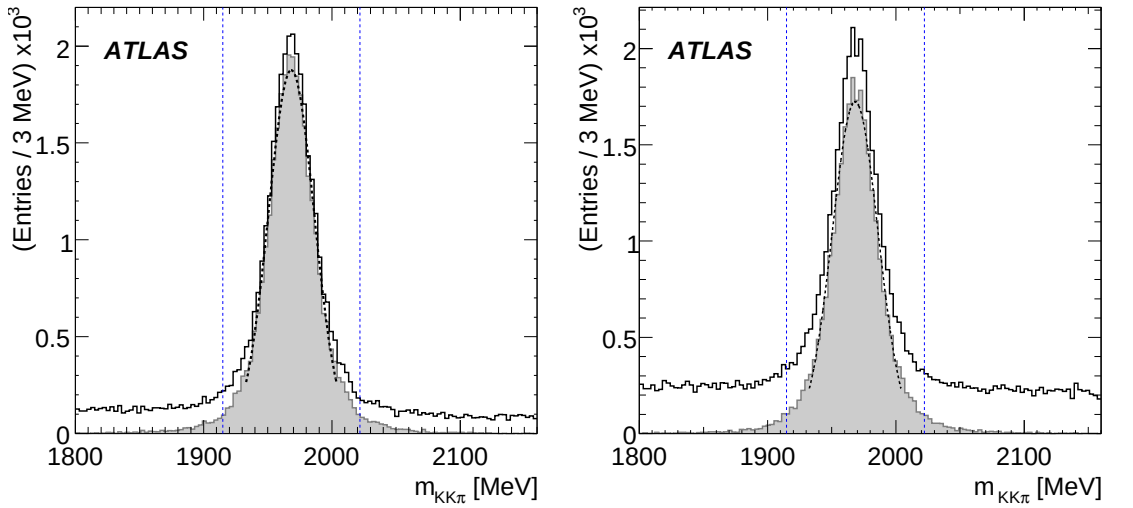

(a) $B_s^0 \to D_s^- \pi^+$ (b) $B_s^0 \to D_s^- a_1^+$

Figure 8: Reconstructed mass $m_{KK\pi}$ for all combinations within the signal sample (black line) and $KK\pi$ candidates corresponding to a D_s particle from the signal decay in the Monte Carlo truth information (grey filled). The standard deviation obtained from a fit within two standard deviations of a Gaussian function (dashed) to the distribution defines the three standard deviation cut range (vertical dashed). No trigger conditions are applied.

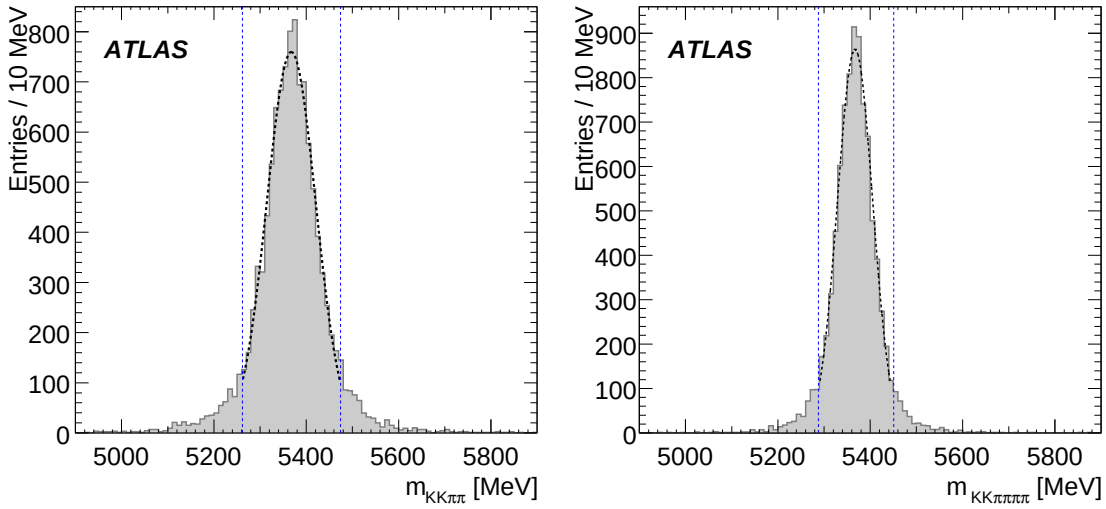

(a) $B_s^0 \to D_s^- \pi^+$ (b) $B_s^0 \to D_s^- a_1^+$

Figure 9: $m_{KK\pi\pi}$ (a) and $m_{KK\pi\pi\pi\pi}$ (b) reconstructed mass and fit of a Gaussian function to the distribution. Each $KK\pi\pi$ ($KK\pi\pi\pi\pi$) candidate displayed corresponds to a B_s particle in the Monte Carlo truth information. The two standard deviation cut range is shown by the vertical dashed lines. No trigger chain applied.

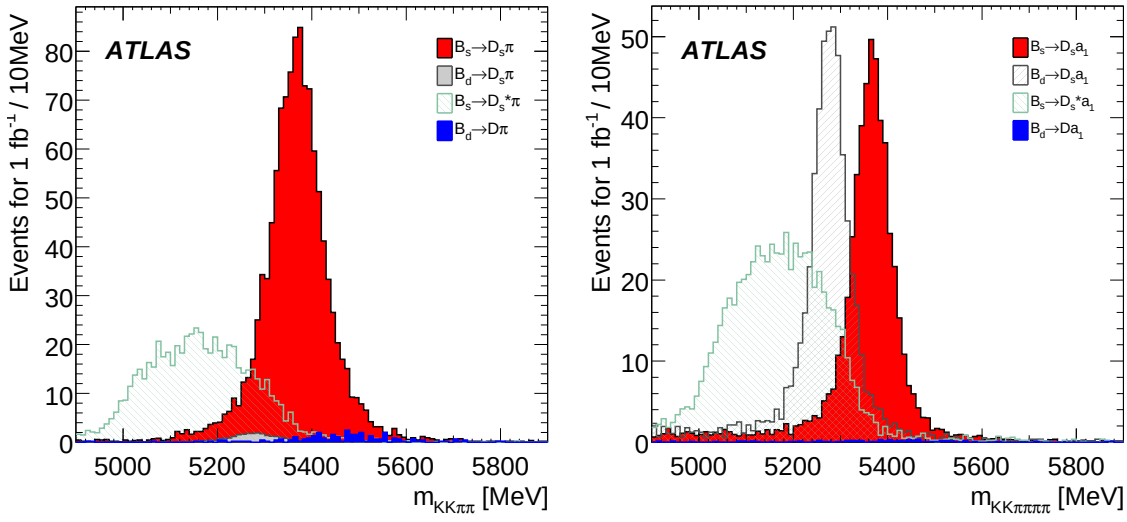

(a) $B_s^0 \to D_s^- \pi^+$ (b) $B_s^0 \to D_s^- a_1^+$

Figure 10: $m_{KK\pi\pi}$ (a) and $m_{KK\pi\pi\pi\pi}$ (b) reconstructed mass for signal and background channels. In (b) the upper limit for the branching fraction of the channel $B_d \to D_s a_1$ is used.

In the case of $B_d^0 \to D_s^+ a_1^-$, there is no measurement of the branching fraction available. The current upper limit is therefore used as a conservative estimate. The similarity to the $B_d^0 \to D_s^+ \pi^-$ channel indicates that the $B_d^0 \to D_s^+ a_1^-$ cross section could be in the same order as the one of the $B_d^0 \to D_s^+ \pi^-$ channel and therefore the $B_d^0 \to D_s^+ a_1^-$ contribution in Fig. 10 (b) could be much smaller.

The $B_s \to D_s^* \pi$ and $B_s \to D_s^* a_1$ channels are treated as a background source, since the momentum and hence the lifetime estimation for this decay is flawed due to the missing photon from the decay of the D_s^*.

5.2.2 Combinatorial Background

The limited statistics of the combinatorial background samples (e.g. 242 150 events for $b\bar{b} \to \mu 6X$) do not allow us to give a reasonable estimate for the signal to background ratio. This ratio as well as kinematic properties of the combinatorial background, like the shape of the proper time distribution will be studied once early data are available.

5.3 Tagging Results

Soft muon tagging is applied on all available simulated data of the two hadronic signal channels $B_s^0 \to D_s^- \pi^+$ and $B_s^0 \to D_s^- a_1^+$. Table 11 shows the number of events, the tagging efficiency and the wrong tag fractions. The tagging efficiency corresponds to the fraction of events where muon candidates have been successfully reconstructed. The events with at least one muon are separated into events with a good tag and events with a wrong tag resulting in a wrong tag fraction.

Comparing the results for all simulated events between the two signal channels, the difference in the wrong tag fraction is of the order 1 % due to the different kinematical topology. As the RoI trigger applies a p_T cut of 1.4 GeV on all reconstructed tracks, low p_T B_s^0 mesons are rejected leading to an increased wrong tag fraction for the triggered events (see Fig. 6(c) and 6(d)). After event reconstruction overall wrong tag fractions of $\omega = 22.30^{+0.56}_{-0.55}$ % for the channel $B_s^0 \to D_s^- \pi^+$ and $\omega = 23.31^{+0.56}_{-0.55}$ % for the channel $B_s^0 \to D_s^- a_1^+$ are observed. Effects of mixing are included as described in Section 4.1.

Table 11: Tagging efficiencies and wrong tag fractions for the signal channels $B_s^0 \to D_s^- \pi^+$ and $B_s^0 \to D_s^- a_1^+$ are shown for three different stages: all simulated events, all triggered events passing the LVL1 muon trigger and the LVL2 RoI trigger, and finally the numbers for the reconstructed events. The errors are statistical only.

Process	Type of Events	Number of Events	Tagging Efficiency [%]	Wrong Tag Fraction [%]
$B_s^0 \to D_s^- \pi^+$	all events	88450	96.08 ± 0.07	20.29 ± 0.14
	triggered	21613	98.77 ± 0.07	22.96 ± 0.29
	reconstructed	5687	$98.79^{+0.14}_{-0.15}$	$22.30^{+0.56}_{-0.55}$
$B_s^0 \to D_s^- a_1^+$	all events	98450	95.93 ± 0.06	21.05 ± 0.13
	triggered	27118	98.55 ± 0.07	23.91 ± 0.26
	reconstructed	5757	$98.47^{+0.16}_{-0.17}$	$23.31^{+0.56}_{-0.55}$

6 Determination of Δm_s

6.1 Methods for the Determination of Δm_s and its Measurement Limits

For the determination of the B_s^0 oscillation frequency the maximum likelihood method is used. The likelihood $\mathscr{L}$ is a function of the proper time t and the mixing state μ, parametrised by Δm_s and $\Delta\Gamma_s$, applied to five classes of events simultaneously: mixed and unmixed B_s^0, mixed and unmixed B_d^0, and background with lifetime but no mixing. The B_s^0 and B_d^0 classes have characteristic wrong tag fractions ω, which are determined on event-by-event basis as described previously. By maximising the likelihood $\mathscr{L}$ for a given event sample one can then extract the model parameters.

For obtaining the $5\,\sigma$ discovery and 95% exclusion measurement limits on Δm_s the amplitude fit method is used because the maximum likelihood method was found to have some disadvantages in that case [5]. The estimation of the maximum value of Δm_s measurable with the ATLAS detector is using B_s^0 candidates from the $B_s^0 \to D_s^- \pi^+$ and $B_s^0 \to D_s^- a_1^+$ hadronic channels. The numbers of reconstructed events after applying the trigger selection (L1_MU06 and LVL2 RoI) and the B_s^0 selection cuts as well as the expected numbers for an integrated luminosity of 10 fb^{-1}are given in Table 12 for all signal and background channels. The effective cross-sections for the various processes can be found in Table 1. Significant background comes from the $\bar{B}_d^0 \to D_s^- \pi^+/a_1^+$ and $B_s^0 \to D_s^{*-} \pi^+/a_1^+$ channels, and from the combinatorial background. Due to limited sample size the estimation of the combinatorial background is very approximate.

The relative fractions of the signal and the background contributions will be determined by a fit of mass shape templates to the reconstructed B_s^0 mass distribution employing a wider mass window than used here for the final extraction of Δm_s, similar to the method used by CDF [1]. The mass shape templates will be determined from Monte Carlo mass distributions of the individual channels. Uncertainties in the knowledge of the shapes will be taken into account as part of the systematical uncertainty.

Table 12: Signal and background samples used for the study of B_s^0-$\bar{B}_s^0$ oscillations and number of events as obtained from the analysis as well as expected numbers for an integrated luminosity of 10 fb^{-1}.

Process	Simulated events	Rec. events	Rec. events for 10 fb^{-1}
$B_s^0 \to D_s^- \pi^+$	88 450	5 687	6 657
$B_d^0 \to D_s^+ \pi^-$	43 000	1 814	99
$B_d^0 \to D^- \pi^+$	41 000	23	35
$B_s^0 \to D_s^{*-} \pi^+$	40 500	495	1 116
$B_s^0 \to D_s^- a_1^+$	98 450	5 757	3 368
$B_d^0 \to D_s^+ a_1^-$	50 000	1 385	< 2454
$B_d^0 \to D^- a_1^+$	50 000	49	36
$B_s^0 \to D_s^{*-} a_1^+$	100 000	870	1 052

6.2 Construction of the Likelihood Function

The probability density to observe an initial B_j^0 meson ($j = d,\ s$) decaying at time t_0 after its creation as a $\bar{B}_j^0$ meson is given by

$$p_j(t_0,\ \mu_0) \ = \ \frac{\Gamma_j^2 - (\Delta\Gamma_j/2)^2}{2\Gamma_j}\ \mathrm{e}^{-\Gamma_j t_0}\left(\cosh\frac{\Delta\Gamma_j t_0}{2} + \mu_0 \cos(\Delta m_j t_0)\right) \qquad (1)$$

where $\Delta\Gamma_j = \Gamma^j_{\rm H} - \Gamma^j_{\rm L}$, $\Gamma_j = (\Gamma^j_{\rm H} + \Gamma^j_{\rm L})/2$ and $\mu_0 = -1$.

For the unmixed case (an initial B^0_j meson decaying as a B^0_j meson at time t_0), the probability density is obtained by setting $\mu_0 = +1$ in Eq. 1. Here the small effects of CP violation are neglected. Unlike $\Delta\Gamma_d$, which can be safely set to zero, the width difference $\Delta\Gamma_s$ in the B^0_s-$\bar{B}^0_s$ system could be as much as 20% of the total width [17].

However, the above probability is modified by experimental effects. The probability as a function of μ_0 and the reconstructed proper time t is obtained as the convolution of $p_j(t_0,\, \mu_0)$ with the proper time resolution ${\rm Res}_j(t\,|\,t_0)$:

$$q_j(t,\mu_0) = \frac{1}{N}\int_0^\infty p_j(t_0,\mu_0)\,{\rm Res}_j(t\mid t_0)\,{\rm d}t_0 \tag{2}$$

with the normalisation factor

$$N = \textstyle\int_{t_{\rm min}}^\infty (\int_0^\infty p_j(t',\mu_0)\,{\rm Res}_j(t\mid t')\,{\rm d}t')\,{\rm d}t\ . \tag{3}$$

Here $t_{\rm min}$ = 0.4 ps is the cut on the B^0_s reconstructed proper decay time. Plots in Fig. 11 show the proper time resolutions, which are parametrised with the sum of two Gaussian functions around the same mean value. The widths from the fit are σ_1 = (68.4$\pm$3.3) fs for the core fraction of 53.2% and σ_2 = (157.2$\pm$5.7) fs for the rest of the tail part of the distribution for the $B^0_s \to D^-_s\pi^+$ channel. The values for the $B^0_s \to D^-_s a^+_1$ channel are σ_1 = (72.5$\pm$4.3) fs for the core fraction of (58.0$\pm$6.8) % and σ_2 = (144.7$\pm$7.3) fs for the tail part.

Assuming a fraction ω_j of wrong tags occurring at production and/or decay, the probability becomes

$$\tilde{q}_j(t,\mu) = (1-\omega_j)q_j(t,\mu) + \omega_j q_j(t,-\mu) \tag{4}$$

where μ_0 has been replaced by μ in order to indicate that now we are talking about the experimental observation of same or opposite flavour tags. For each signal channel, the background is composed of oscillating B^0_d mesons, with probability given by Eq. 4, and of non-oscillating combinatorial background, with probability given by Eq. 5, which results from Eq. 1 and Eq. 4 by setting $\Delta m = 0$ and $\Delta\Gamma = 0$:

$${\rm p_{cb}}(t,\mu) = \frac{\Gamma_{\rm cb}}{2}\,{\rm e}^{-\Gamma_{\rm cb}t}\,[1+\mu\,(1-2\omega_{\rm cb})] \tag{5}$$

For a fraction f_{kj} of the j component ($j = s$, d, and combinatorial background cb) in the total sample of type k, one obtains the probability density function

$${\rm pdf}_k(t,\mu) = \sum_{j=s,d,{\rm cb}} f_{kj}\tilde{q}_j(t,\mu)\ . \tag{6}$$

The index $k = 1$ denotes the $B^0_s \to D^-_s\pi^+$ channel and $k = 2$ the $B^0_s \to D^-_s a^+_1$ channel. The likelihood of the total event sample is written as

$$\mathscr{L}(\Delta m_s, \Delta\Gamma_s) = \prod_{k=1}^{N_{\rm ch}}\prod_{i=1}^{N^k_{\rm ev}} {\rm pdf}_k(t_i,\mu_i) \tag{7}$$

where $N^k_{\rm ev}$ is the total number of events of type k, and $N_{\rm ch} = 2$. Each ${\rm pdf}_k$ is properly normalised to unity.

Figure 12 shows how the experimental effects, as parametrised in Eqs. 2, 4, and 6, modify the distribution of the proper time t of a Monte Carlo data sample.

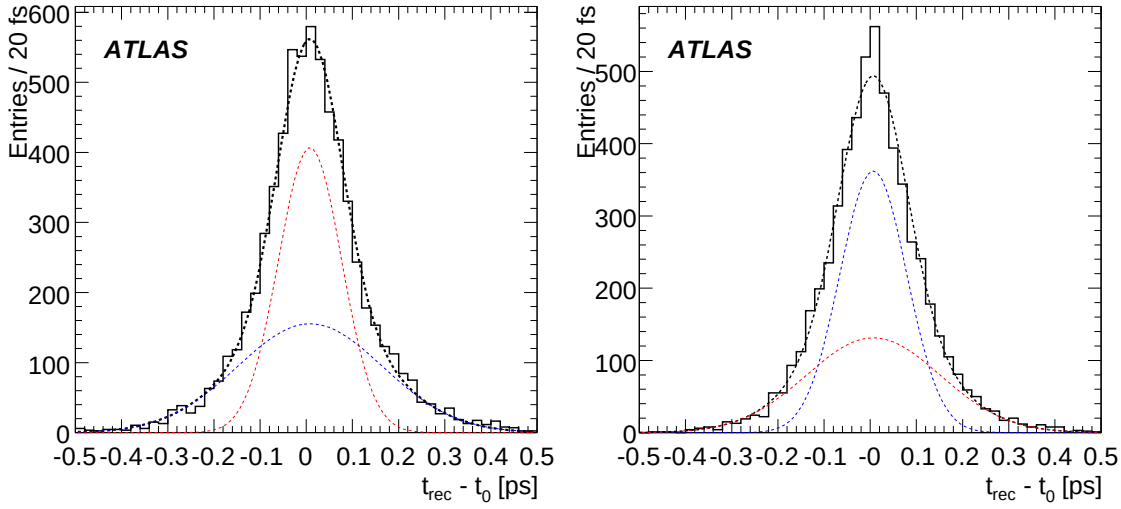

(a) $B_s^0 \to D_s^- \pi^+$ (b) $B_s^0 \to D_s^- a_1^+$

Figure 11: The resolution σ_t of the proper time of simulated B_s^0 fitted with two Gaussian functions (dashed lines). Both Gaussian functions use a common mean value.

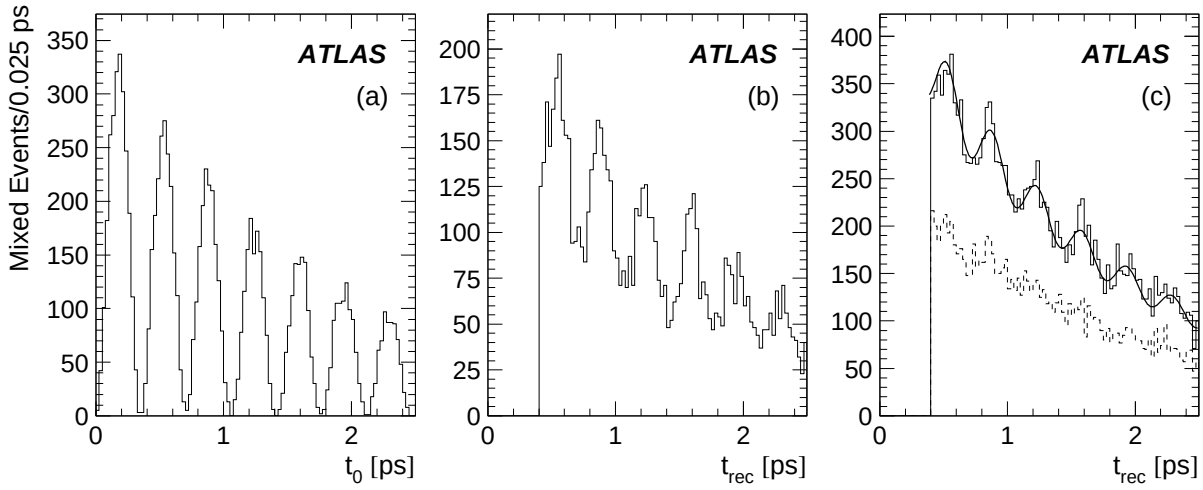

Figure 12: A sequence of plots showing how a true B_s^0 oscillation signal with $\Delta m_s^{gen} = 17.77$ ps^{-1} (a) is diluted first by the effect of a finite proper time resolution (b) and then by adding background events and including the effect of wrong tags (c). The plots contain samples of events equivalent to 10 fb^{-1} of integrated luminosity. They were generated using the Monte Carlo method described in Section 6.3. Only the case of mixed events is shown. For illustration a χ^2-fit of the function $C\exp(-t/\tau)(1-D\cos(\Delta m_s t))$ is overlaid to the solid histogram in (c), where D can be interpreted as the combined dilution factor: $D \approx 0.1$ here. Note that this is different from the unbinned maximum likelihood fit to the total event sample of mixed and unmixed events which is actually used to derive results in this study. The dashed histogram in (c) describes the contribution from all background sources.

6.3 Monte Carlo Data Sample

For the amplitude fit method a simplified Monte Carlo method is applied to generate a B_s^0 sample using the following input parameters: for each signal channel k the number of reconstructed signal events $N_{\rm sig}^{(k)}$ for an integrated luminosity of 10 fb^{-1} and the number of background events $N_{B_{d,s}^0}^{(k)}$ from $B_{d,s}^0$ decays is given in Table 12. For the combinatorial background the ratio $N_{\rm sig}^{(k)}/N_{\rm cb}^{(k)}$ is taken to be 1. The wrong tag fraction is assumed to be the same for both B_s^0 and B_d^0 mesons in a specific signal channel ($\omega_s = \omega_d$), however, the values are slightly different for the two signal channels (see Table 11).

A Monte Carlo sample with $N_{\rm sig} = N_{\rm sig}^{(1)} + N_{\rm sig}^{(2)}$ signal events oscillating with a given frequency Δm_s (e.g. Δm_s = 100 ps^{-1}, which is far off the expected value for Δm_s), together with $N_{B_{d,s}^0} = N_{B_{d,s}^0}^{(1)} + N_{B_{d,s}^0}^{(2)}$ background events oscillating with frequency $\Delta m_{d,s}$ and $N_{\rm cb} = N_{\rm cb}^{(1)} + N_{\rm cb}^{(2)}$ combinatorial events (no oscillations) is generated according to Eq. 1.

The uncertainty on the measurement of the transverse decay length, $\sigma_{d_{xy}}$ (see Fig. 13), and the true value of the g-factor g_0 ($g := m/p_T$) as seen in Fig. 14(a), are generated randomly according to the distributions obtained from the simulated samples, fitted with appropriate combinations of Gaussian and exponential functions. For the $B_s^0 \to D_s^- a_1^+$ channel the true p_T^0 distribution shown in Fig. 14(b) is fitted with a combination of a parabola function in the low p_T^0 region and a sum of two exponential functions in the high p_T^0 region. The g_0 values are obtained by converting generated p_T^0 values at random.

From the computed true decay length, $d_{xy}^0 = t_0/g_0$, the corresponding reconstructed decay length is generated as $d_{xy} = d_{xy}^0 + \sigma_{d_{xy}} \cdot (\mu_{dxy} + S_{d_{xy}}\Omega)$. t_0 is the proper time of the generated B_s. $S_{d_{xy}}$ is the width and μ_{dxy} the mean value of the Gaussian shape of the pull of the transverse decay length $\frac{d_{xy}-d_{xy}^0}{\sigma_{d_{xy}}}$ shown in Fig. 15. The fitted values are $S_{d_{xy}} = 1.099 \pm 0.011$ and $\mu_{dxy} = (8.76 \pm 1.47) \cdot 10^{-2}$ for the $B_s^0 \to D_s^- \pi^+$ channel respectively $S_{d_{xy}} = 1.113 \pm 0.011$ and $\mu_{dxy} = (5.40 \pm 1.48) \cdot 10^{-2}$ for the $B_s^0 \to D_s^- a_1^+$ channel. The reconstructed g-factor is generated as $g = g_0 + g_0\mu_g + g_0 S_g \Omega'$. The distribution of the fractional g-factor $\frac{g-g_0}{g_0}$ as shown in Fig. 16 is fitted with a Gaussian resulting in a width of $S_g = (0.89 \pm 0.01) \cdot 10^{-2}$ and a mean value of $\mu_g = (0.27 \pm 0.12) \cdot 10^{-3}$ for the $B_s^0 \to D_s^- \pi^+$ channel respectively $S_g = (0.82 \pm 0.01) \cdot 10^{-2}$ and $\mu_g = (0.56 \pm 0.11) \cdot 10^{-3}$ for the $B_s^0 \to D_s^- a_1^+$ channel. Both Ω and Ω' are random numbers distributed according to the normal distribution. From the transverse decay length and g-factor, the reconstructed proper time is then computed as $t = g d_{xy}$. The probability for the event to be mixed or unmixed is determined from the t_0 and Δm_s (or Δm_d) values using the expression $(1 - \cos(\Delta m_j t_0)/\cosh(\Delta\Gamma_j t_0/2))/2$ which is left from Eq. 1 after the exponential part has been separated.

For a fraction of the events, selected at random, the state is interchanged between mixed and unmixed, according to the wrong tag fraction $\omega_{\rm tag}$. Half of the combinatorial events are added to the mixed events and half to the unmixed events.

For the exclusive $B_{d,s}^0$ background channels as well as the combinatorial background, the reconstructed proper time is generated assuming that it has the same distribution as the one for signal B_s^0 mesons coming from the $D_s^- \pi^+$ and $D_s^- a_1^+$ sample respectively, no mixing included.

The Δm_s measurement limits are obtained applying the amplitude fit method [5] to the sample generated as described in the previous section. According to this method a new parameter, the B_s^0 oscillation amplitude $\mathcal{A}$, is introduced in the likelihood function by replacing the term '$\mu_0 \cos\Delta m_s t_0$' with '$\mu_0 \mathcal{A} \cos\Delta m_s t_0$' in the B_s^0 probability density function given by Eq. 1. The new likelihood function, similar to Eq. 7, again includes all experimental effects. For each value of Δm_s, this likelihood function is minimized with respect to $\mathcal{A}$, keeping all other parameters fixed, and a value $\mathcal{A} \pm \sigma_{\mathcal{A}}^{\rm stat}$ is obtained. One expects, within the estimated uncertainty, $\mathcal{A} = 1$ for Δm_s close to its true value, and $\mathcal{A} = 0$ for Δm_s

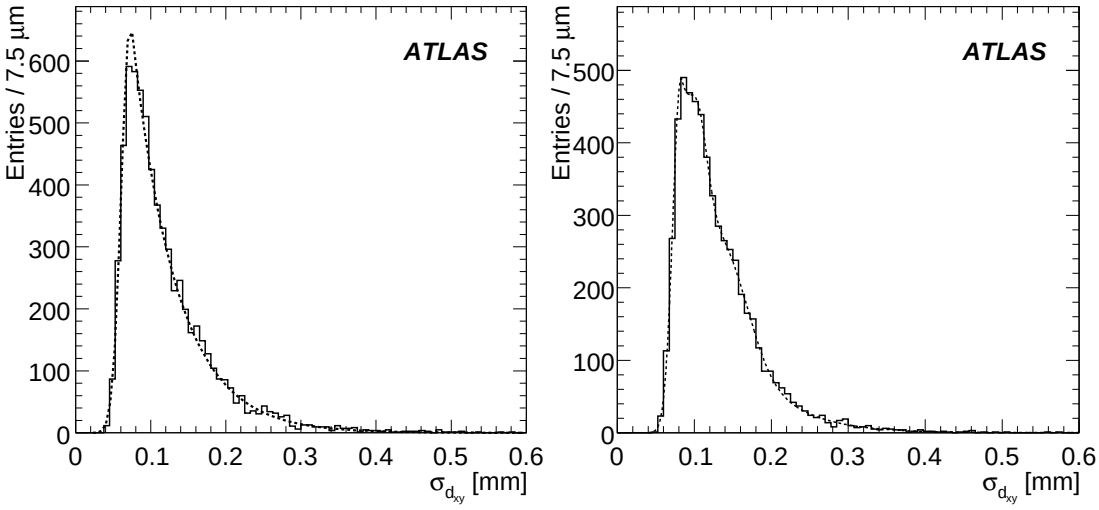

(a) $B_s^0 \to D_s^- \pi^+$ (b) $B_s^0 \to D_s^- a_1^+$

Figure 13: The uncertainty on the measurement of the transverse decay length, $\sigma_{d_{xy}}$ including trigger selection.

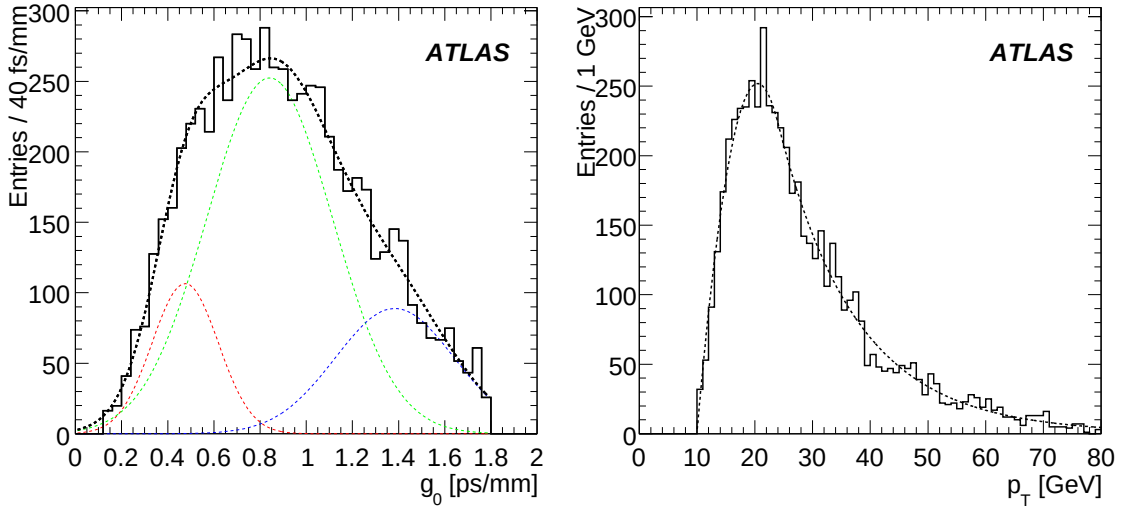

(a) $B_s^0 \to D_s^- \pi^+$ (b) $B_s^0 \to D_s^- a_1^+$

Figure 14: The true value of the g-factor $g_0 = t_0/d_{xy}^0$ of simulated B_s^0 from the $B_s^0 \to D_s^- \pi^+$ sample (a) fitted with the sum of three Gaussian functions (dashed lines) and the true transverse momentum distribution p_T^0 of simulated B_s^0 from the $B_s^0 \to D_s^- a_1^+$ sample (b) including trigger selection.

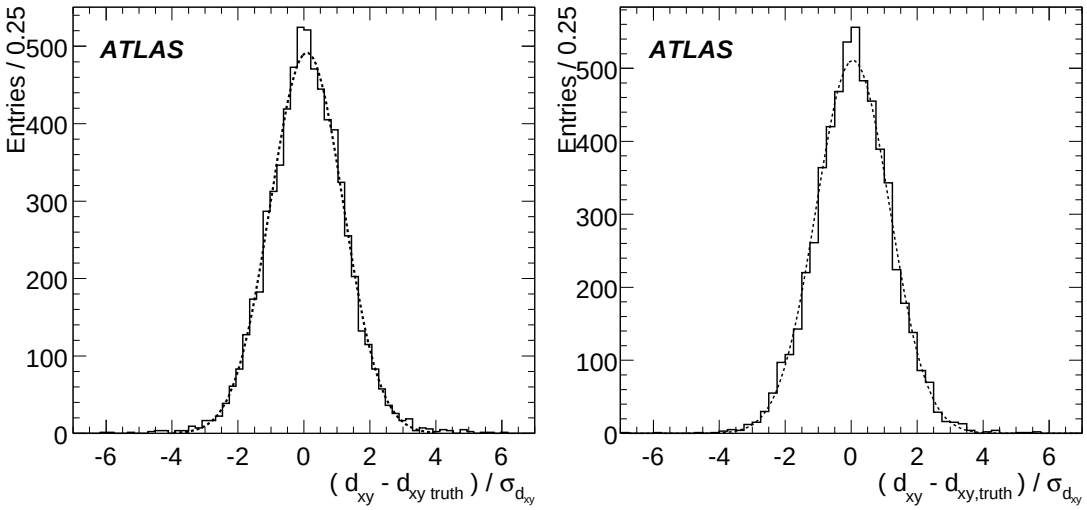

(a) $B_s^0 \to D_s^- \pi^+$ (b) $B_s^0 \to D_s^- a_1^+$

Figure 15: The pull of the measurement of the transverse decay length, $\frac{d_{xy}-d_{xy}^0}{\sigma_{d_{xy}}}$ and fit of a Gaussian function (dashed) to the distribution including trigger selection.

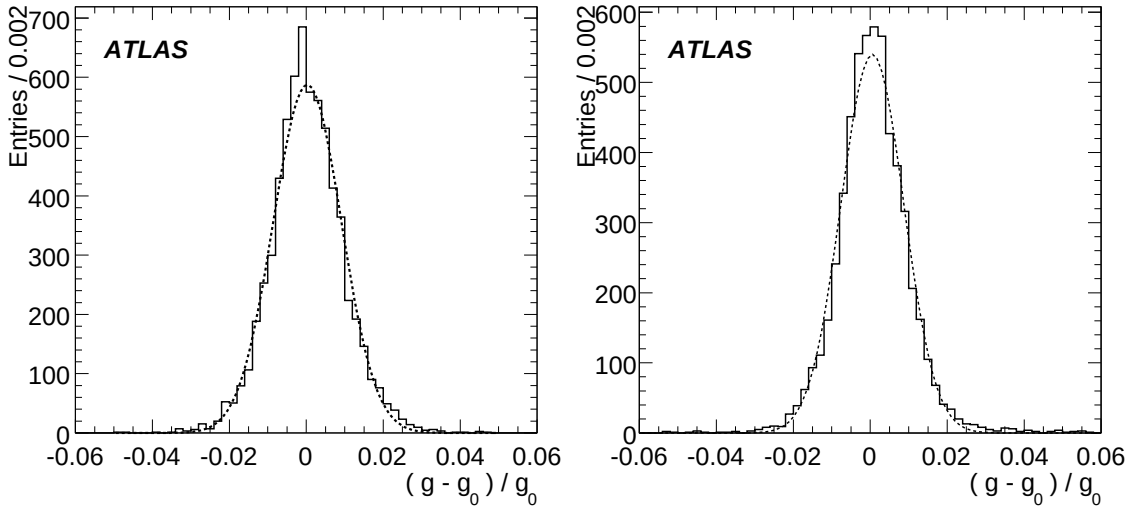

(a) $B_s^0 \to D_s^- \pi^+$ (b) $B_s^0 \to D_s^- a_1^+$

Figure 16: The fractional resolution of the g-factor $\frac{g-g_0}{g_0}$ of simulated B_s^0 fitted with a single Gaussian function including trigger selection.

far from the true value. A five standard deviation measurement limit is defined as the value of Δm_s for which $1/\sigma_{\mathscr{A}} = 5$, and a sensitivity at 95% C.L. as the value of Δm_s for which $1/\sigma_{\mathscr{A}} = 1.645$. Limits are computed with the statistical uncertainty $\sigma^{\text{stat}}_{\mathscr{A}}$. A detailed investigation on the systematic uncertainties $\sigma^{\text{syst}}_{\mathscr{A}}$, which affects the measurement of the B^0_s oscillation, is presented in [18].

6.4 Extraction of the Δm_s Sensitivity

For the nominal set of parameters (as defined in the previous sections), $\Delta\Gamma_s = 0$ and an integrated luminosity of 10 fb^{-1}, the amplitude $\pm 1\sigma^{\text{stat}}_{\mathscr{A}}$ is plotted as a function of Δm_s in Fig. 17(a). The 95% C.L. sensitivity to measure Δm_s is found to be 29.6 ps^{-1}. This value is given by the intersection of the dashed line, corresponding to 1.645 $\sigma^{\text{stat}}_{\mathscr{A}}$, with the horizontal line at $\mathscr{A} = 1$.

From Fig. 17(b), which shows the significance of the measurement $S(\Delta m_s) = 1/\sigma_{\mathscr{A}}$ as a function of Δm_s, the 5σ measurement limit is found to 20.5 ps^{-1}.

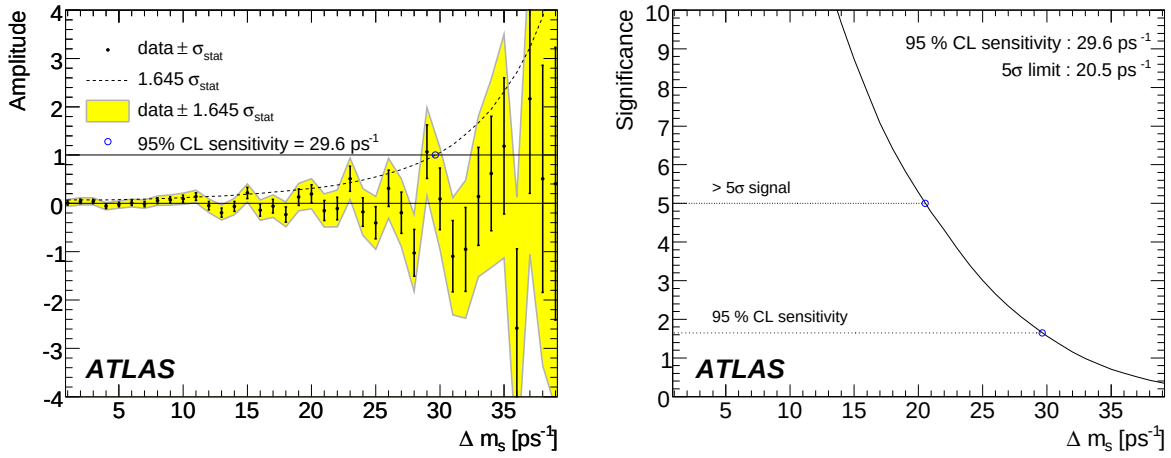

(a) Amplitude vs. Δm_s

(b) Significance vs. Δm_s

Figure 17: The B^0_s oscillation amplitude (a) and the measurement significance (b) as a function of Δm_s for an integrated luminosity of 10 fb^{-1} for a specific Monte Carlo experiment with Δm_s^{gen} = 100 ps^{-1} .

The dependence of the Δm_s measurement limits on the integrated luminosity is shown in Fig. 18(a), with the numerical values given in Table 13.

The dependence of the Δm_s measurement limits on $\Delta\Gamma_s/\Gamma_s$ is determined for an integrated luminosity of 10 fb^{-1}, other parameters having their nominal value. The $\Delta\Gamma_s/\Gamma_s$ is used as a fixed parameter in the amplitude fit method. As shown in Fig. 18(b) no sizeable effect is seen up to $\Delta\Gamma_s/\Gamma_s \sim 30\%$.

6.5 Extraction of the Δm_s Measurement Precision

Whereas the Δm_s measurement limits are obtained by using the amplitude method (see previous section), in case of the presence of an oscillation signal in the data the value of the oscillation frequency Δm_s and its precision are determined by minimising the likelihood (given by Eq. 7) with respect to Δm_s. In this fit $\Delta\Gamma_s$ is fixed to 0, because a study has shown that the systematic uncertainties resulting from varying $\Delta\Gamma_s/\Gamma_s$ in the range 0 to 0.2 (suggested by the present uncertainty) are practically negligible.

An example of the likelihood function is given in Fig. 19(a), in which the Δm_s^{gen} in the Monte Carlo sample has been set to the value measured by CDF for illustration. From this type of graphs the precision

Table 13: The dependence of Δm_s measurement limits on the integrated luminosity $\mathscr{L}$.

$\mathscr{L}$ [fb^{-1}]	5 σ limit [ps^{-1}]	95% C.L. sensitivity [ps^{-1}]
3	14.5	25.0
5	17.0	27.0
10	20.5	29.6
20	23.7	32.0
30	25.3	33.2
40	26.4	34.1

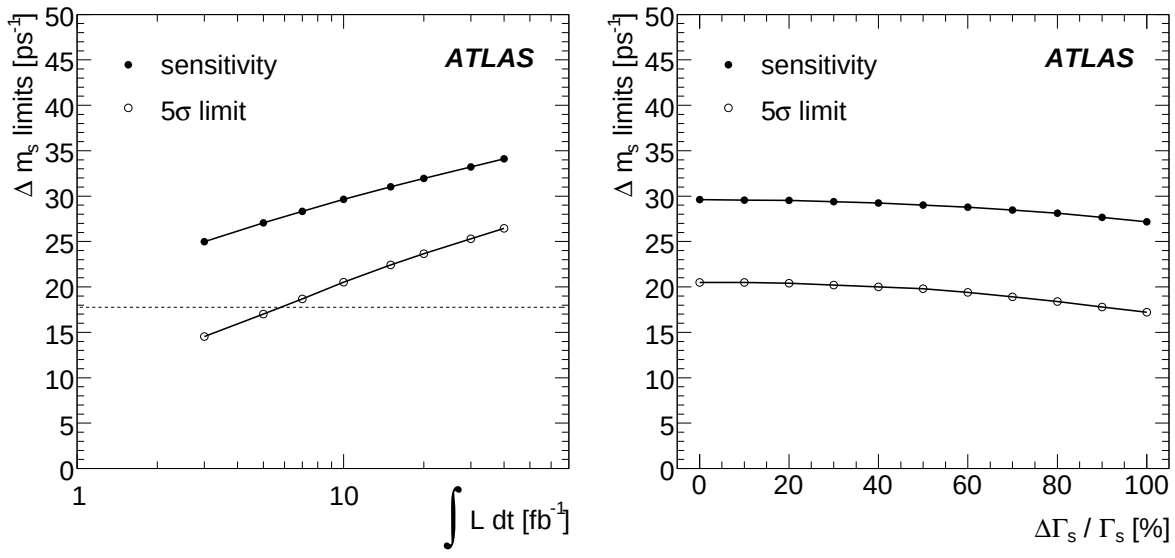

(a) Δm_s limits vs. $\int L\,dt$

(b) Δm_s limits vs. $\Delta\Gamma_s/\Gamma_s$

Figure 18: The dependence of Δm_s measurement limits (a) on the integrated luminosity and (b) on $\Delta\Gamma_s/\Gamma_s$ for an integrated luminosity of 10 fb^{-1}. The dashed horizontal line in (a) denotes the CDF measurement.

of the measurement of Δm_s is extracted and plotted in Fig. 19(b) as a function of the integrated luminosity for three values of Δm_s^{gen}.

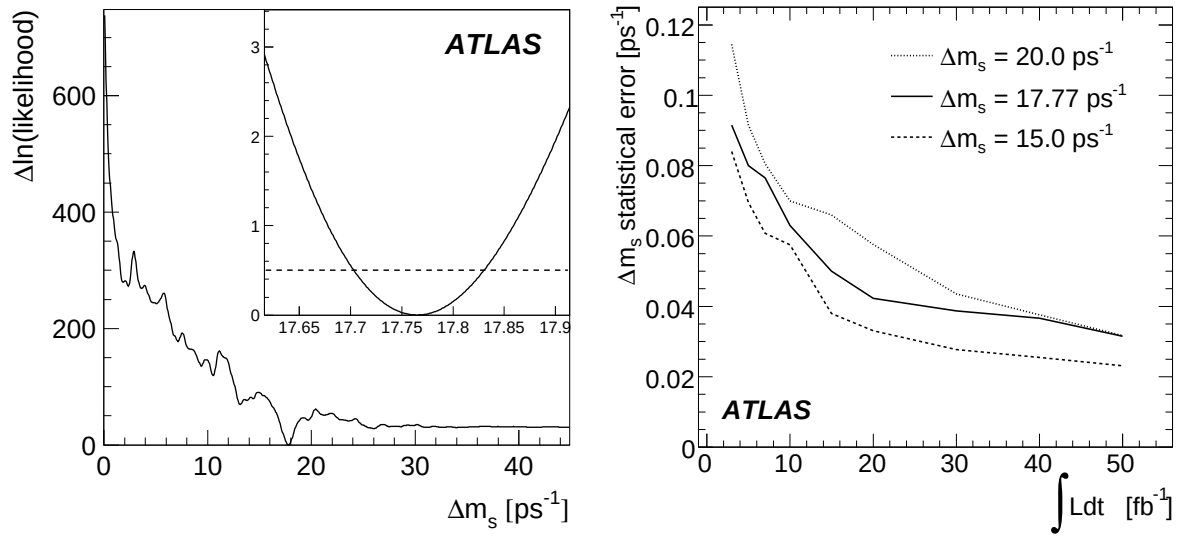

(a) $\Delta\ln(\text{likelihood})$ vs. Δm_s

(b) $\sigma_{\text{stat}}(\Delta m_s)$ vs. $\int L\,dt$

Figure 19: (a) The negative natural logarithm of the likelihood for a specific Monte Carlo data sample for an integrated luminosity of 10 fb^{-1} and a true value of Δm_s^{gen} = 17.77 ps^{-1}. The inset shows a zoom around the minimum. (b) The statistical error $\sigma_{\text{stat}}(\Delta m_s)$ as a function of the integrated luminosity for values of Δm_s^{gen} of 15, 17.77 and 20 ps^{-1}. For comparison: the CDF statistical error on their Δm_s measurement is 0.10 ps^{-1}.

6.6 Discussion of Results

In this note it is shown that with an integrated luminosity of 10 fb^{-1} ATLAS is able to verify the CDF measurement of $\Delta m_s = (17.77 \pm 0.10\,(\text{stat}) \pm 0.07\,(\text{sys}))\,\text{ps}^{-1}$ at the five standard deviation level. For these parameters the statistical error on Δm_s is calculated to be about 0.065 ps^{-1}.

In a preceding study [18] it was found that over a wide range of values for Δm_s and integrated luminosity the systematic uncertainty on the measured value of Δm_s was smaller by at least a factor of 10 compared to the statistical uncertainty. The list of contributions to that systematic error estimation included the wrong tag fraction with a relative error of 5% compared to 2.5% found in this study. For the reasons mentioned above, the evaluation of systematic effects has not been repeated here. The study of the effect of varying $\Delta\Gamma_s$ (as explained in the previous section) is new, but the contribution to the systematic uncertainty is also very small.

Systematic uncertainties on the overall trigger efficiencies mainly effect the statistics available for the analysis. However, an important systematic effect for the Δm_s measurement would be introduced in case different trigger efficiencies for positively and negatively charged muons are observed. In order to constrain this effect, dimuon events from a calibration channel like $B^+ \to J/\psi K^+$ with $J/\psi \to \mu^+\mu^-$ which are triggered by a single muon trigger could be used.

Clearly LHCb can measure Δm_s more precisely than ATLAS ($\sigma_{\text{stat}}(\Delta m_s) \sim 0.01$ ps^{-1} with 2 fb^{-1} of data [19]), but the Δm_s measurement with ATLAS is needed for the simultaneous fit of all parameters of the weak sector of the B_s^0-$\bar{B}_s^0$ system (weak mixing phase ϕ_s, Δm_s, Γ_s and $\Delta\Gamma_s$). This will be performed by

a combined analysis of the channels described in this note and the $B_s^0 \to J/\psi\phi$ channel [20]. The ATLAS measurement is an independent cross-check of the measurements performed by other experiments.

7 Summary and Conclusions

We have studied the capabilities of the ATLAS detector to measure B_s^0 oscillations in pp collisions at 14 TeV using the purely hadronic decay channels $B_s^0 \to D_s^-(\phi\pi^-)\pi^+$ and $B_s^0 \to D_s^-(\phi\pi^-)a_1^+$. For an integrated luminosity of 10 fb^{-1} a Δm_s sensitivity limit of 29.6 ps^{-1} and a five standard deviation measurement limit of 20.5 ps^{-1} is obtained from a likelihood fit employing the amplitude fit method. This result depends only weakly on the lifetime difference $\Delta\Gamma_s$. The trigger is based on a single muon trigger with adjustable muon p_T thresholds between 4 and 10 GeV on all trigger levels and an active search for $D_s \to \phi\pi$ decays by the High Level Trigger. For 10^{31} cm^{-2}s^{-1} we will be able to afford a muon trigger with the loosest p_T threshold combined with a FullScan $D_s \to \phi\pi$ search. For 10^{32} cm^{-2}s^{-1}, we will need to increase the muon p_T threshold to 6 GeV and possibly employ the RoI-based LVL2 trigger. In both cases, the trigger rates can be kept at an acceptable level. For higher luminosities, we need to implement additional constraints in the HLT in order to reduce the event output rates further.

The offline event reconstruction searches for the hadronic decay of the B_s^0 and requires a muon with a minimum p_T of 6 GeV for each event. While the flavour of the B_s^0 at decay time is determined from the charge of the D_s particle, the identification of the initial B_s^0 flavour at production time is extracted from the charge of the soft muon in the event, taking effects of B_s^0 mixing into account. An overall tagging efficiency of $98.8 \pm 0.2\%$ and $98.5 \pm 0.2\%$ as well as average wrong tag fractions of $22.3 \pm 0.6\%$ and $23.3 \pm 0.6\%$ for the $B_s^0 \to D_s^-\pi^+$ and the $B_s^0 \to D_s^- a_1^+$ channels, respectively, are obtained.

About 100000 Monte Carlo events of each sample have been produced without B_s^0 oscillations. Monte Carlo events for several exclusive B_s^0 and B_d^0 background channels as well as for inclusive background like $b\bar{b} \to \mu X$ and $c\bar{c} \to \mu X$ have been used. The hadronic decay of the signal side B_s^0 is reconstructed constraining the masses of intermediate particles in the decay chain. A B_s^0 mass resolution of 52.8 ± 0.7 MeV and 40.8 ± 0.5 MeV is obtained and after the application of all analysis cuts, 6657 and 3368 events are expected for an integrated luminosity of 10 fb^{-1} for the $B_s^0 \to D_s^-\pi^+$ and the $B_s^0 \to D_s^- a_1^+$ decay channels, respectively. We have considered several exclusive background channels, contributing to the background inside the B_s^0 mass window. The $B_d^0 \to D^-\pi^+/a_1^+$ channels hardly contribute (percent level of the signal), but the $B_s^0 \to D_s^{*-}\pi^+/a_1^+$ make a considerable contribution of about 16% ($B_s^0 \to D_s^-\pi^+$) and 31% ($B_s^0 \to D_s^- a_1^+$). While the $B_d^0 \to D_s^-\pi^+$ channel is expected to contribute with about 1.5% relative to the $B_s^0 \to D_s^-\pi^+$ signal, we can only estimate the $B_d^0 \to D_s^- a_1^+$ contribution to be less than about 70% of the $B_s^0 \to D_s^- a_1^+$ signal, given that this decay channel has not yet been observed.

In future, the $B_s^0 \to D_s^{*-}\pi^+/a_1^+$ channels may be considered signal rather than background. An estimate of the combinatorial background is severely limited by the available Monte Carlo event statistics. We plan to use early data to obtain a realistic estimate. For an integrated luminosity of 100 pb^{-1} at 10^{32} cm^{-2}s^{-1} we only expect about 90 events in the $B_s^0 \to D_s^-\pi^+$ and $B_s^0 \to D_s^- a_1^+$ channels, while the $B^+ \to J/\psi(\mu\mu)K^+$ decay channel, which has a large branching ratio, may be used to calibrate the soft muon tagging with early data. On LVL2 the processing time for the $D_s \to \phi\pi$ trigger may be reduced by restricting the track reconstruction to Regions of Interest (RoI), seeded by a LVL1 jet energy trigger. This typically leads to a reduction of the trigger efficiency by a few percent. At an instantaneous luminosity of $2 \cdot 10^{33}$ cm^{-2}s^{-1} several options will be considered to achieve acceptable Event Filter output rates. Besides further constraining the mass windows of the $D_s \to \phi\pi$ trigger, other improvements are obtained by checking for a good reconstruction quality of the D_s vertex or the implementation of a trigger element in the Event Filter which searches for the full B_s^0 decay chain. However, there is an uncertainty of a factor two in the overall $b\bar{b}$ cross-section at the centre-of-mass energy of 14 TeV and therefore the trigger rates may vary.

Due to the achieved sensitivity limit to measure the B_s^0 oscillations we expect to be able to verify the CDF measurement of $\Delta m_s = 17.77 \pm 0.10\,(\text{stat}) \pm 0.07\,(\text{sys})$ ps^{-1} at the five standard deviation level with a statistical error on Δm_s of about 0.065 ps^{-1}. This will provide a reasonable precision which allows us to combine the measurement described in this note with the analysis of the $B_s^0 \to J/\psi\phi$ channel [20] in a simultaneous fit for all parameters of the weak sector of the B_s^0-$\bar{B}_s^0$ system.

8 Acknowledgements

Partial funding for the work described in this note was provided by the the Federal Ministry of Education, Science and Culture, Austria, the German Federal Ministry for Education and Research (BMBF) under grant number 05HA6PS1 as part of the BMBF FSP 101 – ATLAS, by the German Israel Foundation under grant number I-869-56.7, by the Israel Science Foundation under grant number 890015 and by the Science and Technology Facilities Council, UK for the participating scientists from their respective countries.

References

[1] A. Abulencia et al. [CDF Collaboration], Phys. Rev. Lett. **97** (2006) 242003.

[2] V.M. Abazov et al. [D0 Collaboration], Phys. Rev. Lett. **97** (2006) 021802.

[3] M. Battaglia et al. arXiv:hep-ph/0304132 (2003).

[4] ATLAS Collaboration, ATLAS Detector and Physics Performance TDR 15, Vol. 2, (CERN/LHCC/99-15, May 1999).

[5] H.G. Moser and A. Roussarie, Nucl. Instr. Meth. A **384** (1997) 491.

[6] T. Sjöstrand, S. Mrenna and P. Skands, JHEP **05** (2006) 026.

[7] ATLAS Collaboration, Introduction to B Physics, this volume.

[8] W.-M. Yao et al., Journal of Physics G **33** (2006 and 2007 partial update for the 2008 edition) 1+.

[9] H. v. Radziewski, Trigger Considerations for the Measurement of $B_s^0 \to D_s^- a_1^+$ with the ATLAS Experiment, Master's thesis, University of Siegen, 2007 (SI-HEP-2008-05).

[10] ATLAS Collaboration, ATLAS Level-1 Trigger TDR 12, (CERN/LHCC/98-14, June 1998).

[11] C. Schiavi, Real Time Tracking with ATLAS Silicon Detectors and its Applications to Beauty in Hadron Physics, Ph.D. thesis, Genoa University and INFN Genoa, 2005 (CERN-THESIS-2008-028).

[12] ATLAS Collaboration, Triggering on low-p_T muons and di-muons for B Physics, this volume.

[13] P. Nason et al., arXiv:hep-ph/0003142v2 (2001).

[14] ATLAS Collaboration, Muons in the ATLAS Calorimeters: Energy Loss Corrections and Muon Tagging, this volume.

[15] ATLAS Collaboration, Beauty Production Cross Section Measurements with early LHC Data: B-Physics Reference Channel $B^+ \to J/\psi K^+$ and inclusive Methods, this volume.

[16] Upper Tail Probability of Chi-Squared Distribution, CERNLIB - CERN Program Library, routine entry PROB (G100), CERN.

[17] M. Beneke, G. Buchalla and I. Dunietz, Phys. Rev. D **54** (1996), 4419, M. Beneke et al., Phys. Lett. **B459** (1999) 631.

[18] B. Epp, V.M. Ghete, A. Nairz, EPJdirect CN3, SN-ATLAS-2002-015 (2002) 1–23.

[19] S. Barsuk [LHCb Collaboration], LHCb 2005-068 (2005).

[20] ATLAS Collaboration, Physics and performance measurements with mixing induced CPV channels $B_s^0 \to J/\psi\,\phi$ and $B_d^0 \to J/\psi\,K_s^0$, this volume.